



1 **Abstract**

2 Marine atmosphere is usually considered to be a clean environment, while this study indicates  
3 that the near-coast waters of South China Sea (SCS) suffered from even worse air quality than  
4 coastal cities. The analyses were based on concurrent field measurements of target air pollutants  
5 and meteorological parameters conducted at a suburban site (Tung Chung, TC) and a nearby  
6 marine site (Wan Shan, WS) from August to November 2013. The observations showed that the  
7 levels of primary air pollutants were significantly lower at WS than those at TC, while ozone (O<sub>3</sub>)  
8 value was greater at WS. Higher O<sub>3</sub> levels at WS were attributed to the weaker NO titration and  
9 higher O<sub>3</sub> production rate because of stronger oxidative capacity of the atmosphere. However, O<sub>3</sub>  
10 episodes were concurrently observed at both sites under certain meteorological conditions, such  
11 as tropical cyclones, continental anticyclones and sea-land breezes (SLBs). Driven by these  
12 synoptic systems and mesoscale recirculations, the interaction between continental and marine  
13 air masses had profoundly changed the atmospheric composition and subsequently influenced  
14 the formation and redistribution of O<sub>3</sub> in the coastal areas. When continental air intruded into  
15 marine atmosphere, the O<sub>3</sub> pollution was magnified over SCS, and the elevated O<sub>3</sub> (>100 ppbv)  
16 could overspread the sea boundary layer ~8 times the area of Hong Kong. In some cases, the  
17 exaggerated O<sub>3</sub> pollution over the SCS was re-circulated to the coastal inshore by sea breeze,  
18 leading to even aggravating O<sub>3</sub> pollution in coastal cities. The findings are applicable to similar  
19 mesoscale environments around the world where the maritime atmosphere is potentially  
20 influenced by severe continental air pollution.

21 **Key words:** Continental air pollution; Maritime atmosphere; Mesoscale recirculation; Ozone  
22 photochemistry

23

24

## 1 **1 Introduction**

2 Ozone (O<sub>3</sub>) plays a central role in photochemical oxidation processes in the troposphere via  
3 direct reaction, photolysis and the subsequent reactions to produce the hydroxyl radical (Monks  
4 et al., 2015; Seinfeld and Pandis, 2016). As a strong oxidant, O<sub>3</sub> at surface level is recognized to  
5 be a threat to human health (WHO, 2003; Bell et al., 2007) and has a detrimental impact on  
6 vegetation (Fowler et al., 2009) and built infrastructure (Kumar and Imam, 2013). Tropospheric  
7 O<sub>3</sub> is also the third most important greenhouse gas (IPCC, 2014) and is referred to a short-lived  
8 climate pollutant (Shindell et al., 2012).

9 To mitigate O<sub>3</sub> pollution in the troposphere, tremendous efforts from both scientific and  
10 regulatory communities have been made since three decades ago (NRC, 1991; NARSTO, 2000;  
11 Monks et al., 2015). The O<sub>3</sub> levels started to decrease at many locations, such as Jungfrauoch in  
12 Switzerland, Zugspitze in Germany, Mace Head in Ireland, as well as parts of California and  
13 eastern US (Lefohn et al., 2010; Cui et al., 2011; Parrish et al., 2012; Lin et al., 2017). However,  
14 increasing studies showed that surface O<sub>3</sub> was elevated rapidly in East Asia in the last decade  
15 (Ding et al., 2008; Xu et al., 2008; Parrish et al., 2012; Xue et al., 2014; Zhang et al., 2014; Sun  
16 et al., 2016; Lin et al., 2017; Wang et al., 2017a). For example, the observational data revealed  
17 that regional O<sub>3</sub> concentrations increased at a rate of 0.86 ppbv yr<sup>-1</sup> in Pearl River Delta (PRD)  
18 from 2006 to 2011 (Li et al., 2014), at a rate of 0.56 ppbv yr<sup>-1</sup> in Hong Kong from 2005 to 2014  
19 (Wang et al., 2017a), and even at a rate of 1.7-2.1 ppbv yr<sup>-1</sup> (summertime only) at Mount Tai in  
20 central eastern China (Sun et al., 2016).

21 Hong Kong and the adjacent PRD is the most industrialized region along the coast of South  
22 China Sea (SCS), and is suffering from serious O<sub>3</sub> pollution (Zheng et al., 2010; Derwent et al.,  
23 2013; Ling et al., 2013). Numerous studies demonstrated that in addition to long-range transport  
24 (Chan, 2002; Guo et al., 2009; Wang et al., 2009) and local photochemical production (Ding et  
25 al., 2013a), tropical cyclones and mesoscale circulations are conducive to the occurrence of high  
26 O<sub>3</sub> events (Yin, 2004; Huang et al., 2005; Yang et al., 2012; Jiang et al., 2015; Wei et al., 2016).  
27 In a number of studies, tropical cyclone has been considered as the most conducive driver to the  
28 occurrence of O<sub>3</sub> episodes in Hong Kong (Yin, 2004; Ling et al., 2013) for it generally causes

1 peripheral subsidence, stagnation air and inversion layer, which favor the production and  
2 accumulation of O<sub>3</sub>.

3 Mesoscale circulations (*e.g.*, sea-land breezes (SLB) and mountain–valley breezes) also play  
4 important roles in O<sub>3</sub> distribution and transport in the coastal cities like Hong Kong with  
5 complex topography and land cover ( Liu and Chan, 2002; Ding et al., 2004; Lu et al., 2009a;  
6 Guo et al., 2013). For instance, Guo et al. (2013) demonstrated that upslope winds brought  
7 pollutants including O<sub>3</sub> from low-lying areas to the peak of Mt Tai Mo Shan (957 m a.s.l.) in  
8 Hong Kong. Ding et al. (2004) simulated a multi-day SLB related O<sub>3</sub> episode and discussed the  
9 influence of SLB circulation on the transport of oxidant precursors, the residence time and re-  
10 entry of photochemical compounds. Lu et al. (2010) simulated the SLB in the 2003/2004 winter  
11 and revealed that the urbanization of Shenzhen might significantly enhance the sea breeze to the  
12 west of Hong Kong in the early afternoon, which worsened the local air pollution.

13 Both coastal human activities and marine atmospheric cyclic behavior can significantly affect the  
14 air pollution level in coastal urban environments (Adame et al., 2010; Velchev et al., 2011).  
15 Exploring SLBs provides an important way to understand the interaction between continental air  
16 and marine atmosphere which has long been a focus of coastal air quality, global tropospheric  
17 chemistry and climate change research. Surprisingly, few studies investigated SLBs in Hong  
18 Kong though about 70 SLB days per year on average were observed in Hong Kong and the PRD  
19 region (Zhang and Zhang, 1997). Therefore, the association between mesoscale recirculation and  
20 air pollutants over the SCS and subtropical continental region is still not well established, which  
21 seriously limits our understanding on the interplay of continental and marine air masses in this  
22 region. Furthermore, previous O<sub>3</sub> studies carried out in this region neither paid enough attention  
23 to the variations of volatile organic compounds (VOCs, one important group of O<sub>3</sub> precursors)  
24 nor established any field measurements on an island, an ideal site for observation of marine air  
25 mass with less interference from local emissions, for understanding the O<sub>3</sub> pollution around the  
26 coastal region of the SCS (Parrish et al., 1998). So far, only a handful of studies deeply evaluated  
27 the chemical characteristics of air masses under various synoptic systems (Wang et al., 2005;  
28 Guo et al., 2009, 2013; Li et al., 2018).

1 This study aimed to comprehensively characterize interaction between continental anthropogenic  
2 emissions and marine atmosphere over a coastal region of the SCS by concurrent measurements  
3 and in-depth analysis of air pollutants at a marine site over SCS and a suburban site in Hong  
4 Kong. Firstly, the spatial and temporal variations of measurements were described to give an  
5 overall picture of the campaign, as well as to directly evaluate how continental outflows polluted  
6 the marine atmosphere over the SCS. After that, the chemical and meteorological characteristics  
7 of air masses associated with high O<sub>3</sub> concentrations were explored. Finally, the interplay  
8 between the maritime and continental air masses and its influence on regional air quality were  
9 discussed.

## 10 **2 Methodology**

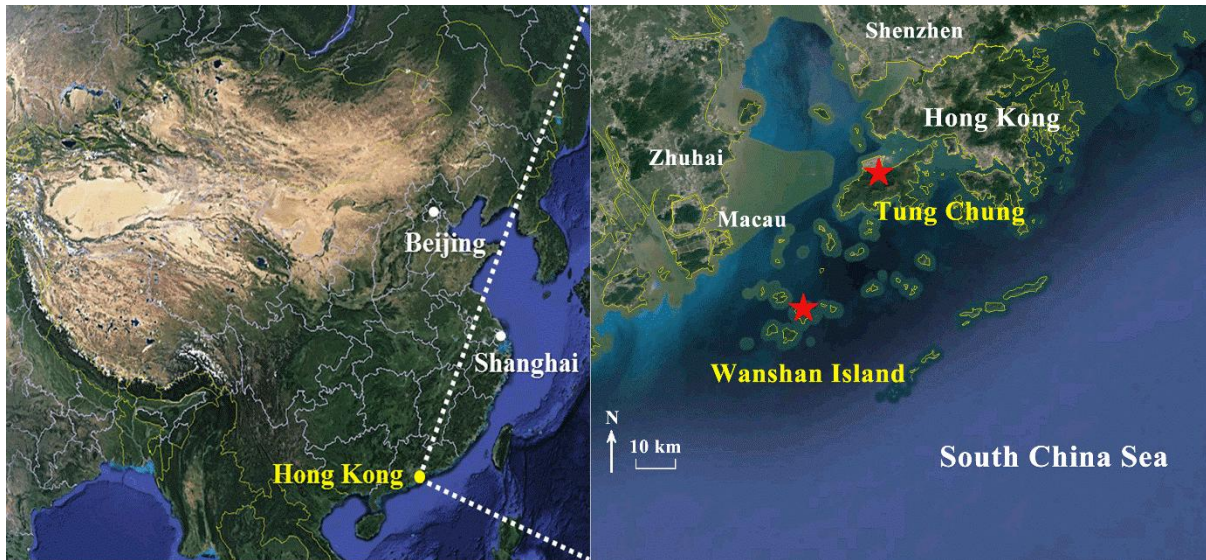
### 11 **2.1 Sampling sites**

12 Field measurements were carried out concurrently at a suburban site and a marine site over SCS  
13 (Figure 1). The suburban Tung Chung (TC, 22.29 ° N, 113.94 ° E) site, part of the Hong Kong  
14 Environmental Protection Department (HKEPD) air quality monitoring network, is located in  
15 southwestern Hong Kong, about 3 km south of the Hong Kong International Airport at Chek Lap  
16 Kok with Hong Kong urban center about 20 km to the southwest and Macau 38 km to the  
17 northeast. It is a newly-developed residential town adjacent to the busy highway and railway  
18 lines. The sampling instruments were installed on the rooftop of a building with a height of 27.5  
19 m a.s.l. More detailed description of the TC site can be found in our previous publications  
20 (Cheng et al., 2010a; Jiang et al., 2010).

21 The marine site, Wan Shan island (WS, 21.93 ° N, 113.73 ° E), is located 40 km southeast of  
22 Zhuhai, and is bounded to the north by the Pearl River Estuary, with a straight distance of about  
23 44 km to TC. WS has an area of 8.1 km<sup>2</sup> and a population of about 3,000 with sparse  
24 anthropogenic emissions at the island. The isolated island features a sub-tropical maritime  
25 climate. The measurement site was set up on the rooftop of the National Marine Environmental  
26 Monitoring Station with a height of about 65 m a.s.l.

27 High O<sub>3</sub> mixing ratios are frequently observed in Hong Kong in late summer and autumn (Ling  
28 et al., 2013) when tropical cyclones and the northeast monsoon prevail, respectively. During this

1 period, WS is right in the downwind direction of TC, which facilitates the study of the  
2 interaction between the inland pollution and the marine environment.



3  
4 **Figure 1.** Locations of the sampling sites (red stars) and the surrounding environment.  
5

## 6 **2.2 Measurement techniques**

### 7 *2.2.1 Measurements of trace gases and meteorological parameters*

8 The sampling campaign was conducted from 10 Aug. to 21 Nov. across late summer and autumn  
9 in 2013. At WS, trace gases (*i.e.*,  $\text{NO}_x$ ,  $\text{O}_3$ ,  $\text{SO}_2$  and  $\text{CO}$ ) were continuously monitored with a time  
10 resolution of 1 minute.  $\text{NO-NO}_2\text{-NO}_x$  was measured using a heated molybdenum  $\text{NO}_2$ -to- $\text{NO}$   
11 converter and a chemiluminescence analyzer (*Thermo Environmental Instruments (TEI), Model*  
12 *42i*) with a range of 0-200 ppbv and a lower detection limit of 0.40 ppbv. It was noteworthy  
13 that the measured  $\text{NO}_x$  might include other oxidized reactive nitrogen that was converted by the  
14 molybdenum. Thus, the  $\text{NO}_x$  concentrations given below were considered the upper limits of  
15 their actual values (Dunlea et al., 2007; Ran et al., 2011).  $\text{O}_3$  was monitored with a commercial  
16 UV photometric analyzer (*TEI, Model 49i*) with a range of 0-0.050 to 200 ppm and a lower  
17 detection limit of 1.0 ppbv.  $\text{SO}_2$  was measured using a pulsed UV fluorescence approach (*TEI,*  
18 *Model 43S*).  $\text{CO}$  was measured by a gas filter correlation, non-dispersive infrared analyzer (*API,*  
19 *Model 300*) with a heated catalytic scrubber to convert  $\text{CO}$  to  $\text{CO}_2$  for baseline determination.

1 Quality assurance and control procedures (*e.g.*, instrumental maintenance and calibration) for  
2 these devices have been described elsewhere (Guo et al., 2009, 2013). Meteorological  
3 parameters, including temperature, relative humidity, solar radiation, wind speed and wind  
4 direction, were routinely monitored by a weather station (Vantage Pro 2 plus, Davis Instruments)  
5 with a time resolution of 5 minutes. At TC, hourly data of the aforementioned trace gases and  
6 meteorological parameters were obtained from the HKEPD  
7 (<http://epic.epd.gov.hk/ca/uid/airdata>). Detailed information of the quality assurance and control  
8 protocols is available in the HKEPD report (HKEPD, 2015).

### 9 2.2.2 Sampling and analysis of VOCs

10 Concurrent VOC samples (*i.e.*, non-methane hydrocarbons (NMHCs) and carbonyls) were  
11 collected on 21 selected days (including both non-O<sub>3</sub> episodes and O<sub>3</sub> episodes) at both sites.  
12 These days were selected on the basis of weather prediction and meteorological data analysis for  
13 potentially high and low O<sub>3</sub> days. An O<sub>3</sub> episode day is the day when the peak one-hour averaged  
14 O<sub>3</sub> mixing ratio exceeds 100 ppbv (Level II of China National Ambient Air Quality Standard).  
15 Please refer to our previous publication for details of this method (Guo et al., 2009).

16 The whole-air samples of NMHCs were collected using 2-L electro-polished stainless steel  
17 canisters. The canisters were cleaned, conditioned and evacuated before being used for  
18 sampling. A metal bellows pump was used to fill up the canisters with sample air over one-hour  
19 integration (with a flow restrictor) to a pressure of 40 psi. Seven one-hour VOC samples (every  
20 two hours during 7:00 – 19:00 inclusive) were collected simultaneously at each site. Intensive  
21 VOC sampling was also carried out at WS in selected seven days (*i.e.*, 3, 4, 9 and 22-25 October) with  
22 eleven one-hour samples (every two hours during 1:00 – 22:00 inclusive). Totally, 311 valid  
23 VOC samples (144 at TC and 167 at WS) were collected in addition to about 5% field blanks and  
24 5% parallel samples for quality assurance purpose. The speciation and abundance of 59 C<sub>2</sub>-C<sub>11</sub>  
25 NMHCs in the canisters were determined by a Model 7100 preconcentrator (Entech Instruments  
26 Inc., California, USA) coupled with an Agilent 5973N gas chromatography-mass selective  
27 detector/flame ionization detector (GC-MSD/FID, Agilent Technologies, USA). The detection  
28 limit of NMHCs was 3 pptv with a measurement precision of 2-5%, and a measurement accuracy

1 of 5%. Detailed information of the analysis system and quality control and quality assurance for  
2 VOC samples can be found elsewhere (Simpson et al., 2010).

3 Carbonyl samples were collected using silica gel filled cartridges impregnated with acidified 2,4-  
4 dinitrophenylhydrazine (DNPH). Air samples were drawn through the cartridge at a flow rate of  
5  $0.8\text{--}0.9\text{ L min}^{-1}$  for 2 hours; the flow rate through the cartridges was monitored with a rotameter  
6 which was calibrated before and after each sampling. An  $\text{O}_3$  scrubber was connected to the inlet  
7 of the DNPH-silica gel cartridge to prevent interference from  $\text{O}_3$ . In total, 227 carbonyl samples  
8 (124 at TC and 103 at WS) were collected with 5 and 6 samples per non- $\text{O}_3$  and  $\text{O}_3$  episode day  
9 (every two hours during 7:00 - 18:00 inclusive), respectively. All cartridges were stored in a  
10 refrigerator at  $4\text{ }^\circ\text{C}$  after sampling. The sampled carbonyl cartridges were eluted slowly with  $<5$   
11 ml of acetonitrile in the direction opposite to sampling flow into a 5-ml brown volumetric flask,  
12 followed by adding acetonitrile to a constant volume of 5 ml. A 20- $\mu\text{l}$  aliquot was injected into  
13 the high performance liquid chromatography (HPLC) system through an auto-sampler. The  
14 operating conditions of the HPLC are shown in Table S1. Typically,  $\text{C}_1\text{--C}_9$  carbonyl compounds  
15 were measured efficiently with a detection limit of  $\sim 0.2$  ppbv.

### 16 **2.3 Observation-based model (OBM)**

17 A photochemical box model coupled with the Master Chemical Mechanism v3.2 (PBM-MCM)  
18 was applied to simulate the  $\text{O}_3$  production at WS and TC for the VOC sampling days. The PBM-  
19 MCM model is a zero-dimension photochemical box model combined with a near explicit  
20 chemical mechanism consisting of 5,900 species and 16,500 reactions, which fully describes the  
21 mechanisms of homogeneous reactions in the atmosphere (Jenkin et al., 1997; Jenkin et al., 2003;  
22 Saunders et al., 2003). The simulation was constrained by hourly data of meteorological  
23 parameters (*i.e.*, temperature and relative humidity) and air pollutants ( $\text{NO}$ ,  $\text{NO}_2$ ,  $\text{CO}$ ,  $\text{SO}_2$  and  
24 51 measured VOCs). Since the sampling interval was two hours for each sample, cubic spline  
25 interpolation was used to derive VOC concentrations at each hour for modeling purpose. Please  
26 see our previous publication for details (Wang et al., 2017a). HONO has been recognized as an  
27 important source of OH, influencing  $\text{O}_3$  formation significantly (Kleffmann, 2007). Since we did  
28 not measure HONO mixing ratios in this study, the average diurnal profiles of HONO observed  
29 at TC in autumn 2011 (Xu et al., 2015) and at a coastal background site (Hok Tsui, HT) in  
30 southeast Hong Kong in autumn 2012 (Zha, 2015) were applied to the photochemical



1 simulations at TC and WS, respectively. Figure S1 shows the average diurnal cycles of HONO at  
2 TC and HT. The use of the aforementioned diurnal profiles might increase the uncertainty of  
3 model simulation. However, we believe that the newly introduced uncertainties could not be too  
4 high, because HONO observations at TC and HT were carried out 2 years and 1 year before the  
5 sampling campaign of this study, respectively. In addition, HT was comparable to WS in aspects  
6 of local emissions (nearly free of anthropogenic emissions), air mass category (mixed continental  
7 and marine air) and location (to the south of Hong Kong and on SCS). It is noteworthy that the  
8 atmospheric physical processes (*i.e.*, vertical and horizontal transport) were not considered in  
9 this model. In addition, the inherent uncertainty of NO<sub>x</sub> measurement mentioned above might  
10 slightly affect the modeling results. The PBM-MCM model has been successfully applied in  
11 previous studies (Cheng et al., 2010b; Lam et al., 2013; Ling et al., 2014). Details of the model  
12 construction can be found in Saunders et al. (2003) and Lam et al. (2013).

#### 13 **2.4 WRF-CMAQ simulation and backward particle release model**

14 In this study, the Weather Research and Forecasting (WRF v3.7.1) model (Skamarock et al.,  
15 2008) was used to simulate vertical and horizontal wind fields for various weather systems  
16 observed in this campaign, and then provided meteorological parameters required by U.S. EPA  
17 Community Multiscale Air Quality (CMAQ v4.7.1) model ([www.epa.gov/cmaq](http://www.epa.gov/cmaq)). CMAQ is a  
18 three-dimensional Eulerian atmospheric chemistry and transport modeling system, which  
19 includes complex physical and chemical processes, such as physical transport and diffuse, gas  
20 and aqueous chemical transformation, and so on; and it can treat multiple pollutants  
21 simultaneously from local to continental scales. A domain system composed of four  
22 nested grids (81, 27, 9, 3 km) was adopted to better suit the simulation of mesoscale weather  
23 systems, as shown in Figure S2. The domain with finest resolution (3 km) covers the Pearl River  
24 Estuary region. Vertically, there were 31 sigma levels for all domains, with the model top fixed  
25 at 50 hPa. The major selected physical schemes invoked in WRF and chemical mechanisms used  
26 in CMAQ are shown in Table S2. The input meteorological data was made using NCEP FNL  
27 (final) data with a horizontal resolution of 1°×1° (<https://rda.ucar.edu/>). In addition, the  
28 geographical data were obtained from the Research Data Archive of National Center for  
29 Atmospheric Research (NCAR) (<http://www2.mmm.ucar.edu/wrf/users/downloads.html>). The  
30 emission inventories (EI) used in this study included the 2000-based Regional Emission

1 Inventory in ASia (REAS) (Kurokawa et al., 2013) and the 2010-based Multi-resolution  
2 Emission Inventory for China (MEIC) (He, 2012), both of which were processed by the Sparse  
3 Matrix Operating Kernel Emission (SMOKE) model. The biogenic emissions were calculated by  
4 the Model of Emissions of Gases and Aerosols from Nature (MEGAN) (Guenther, 2006). The  
5 WRF modelling mainly focused on O<sub>3</sub> episodes with an additional 24hrs' preceding run as spin-  
6 up for each episode, and the integration was conducted separately. In addition, the  
7 spatiotemporal patterns of CO and O<sub>3</sub> were simulated by WRF-CMAQ during two O<sub>3</sub> episodes  
8 (see section 3.4). The time series of the simulations and observations of CO and O<sub>3</sub> are shown in  
9 Figure S3. Also, Table S3 gives the index of agreements (IOAs) between the simulated and  
10 observed meteorological parameters and air pollutants. Within the range of 0 – 1, higher IOAs  
11 represent better agreement between the simulated and observed values (Willmott, 1982). Here,  
12 IOA was between 0.51 and 0.84 for the simulation of meteorological parameters. Furthermore, it  
13 was not lower than 0.50 for primary air pollutants, and reached 0.81 for O<sub>3</sub> simulation at both  
14 sites. The model performances were comparable to those reported in previous studies (Cabaraban  
15 et al., 2013; Wang et al., 2015). Therefore, we accepted the modeling results, in view of the fact  
16 that the simulations were only used to qualitatively indicate the interactions between the  
17 continental and marine air in this study.

18 Backward particle release simulations were carried out using HYSPLIT model (Stein et al., 2015)  
19 for episode days at WS and TC sites during the entire sampling period (Draxler and Rolph, 2003).  
20 The backward particle release simulation, which considers the dispersion processes in the  
21 atmosphere, is capable of identifying the history of air masses (Guo et al., 2009; Ding et al.,  
22 2013a, 2013b). In this work, we applied the model following a method developed by Ding et al.  
23 (2013a).

## 24 **3 Results and Discussion**

### 25 **3.1 Spatio-temporal variations**

26 Table 1 summarizes the meteorological conditions and chemical species observed at WS and TC.  
27 Lower temperature ( $25.7 \pm 0.1^\circ\text{C}$ ) and higher relative humidity ( $82.8 \pm 0.4\%$ ) were recorded at the  
28 marine site (WS) compared to the suburban site (TC) ( $p < 0.01$ ) (temperature:  $26.7 \pm 0.1^\circ\text{C}$  and  
29 relative humidity:  $67.7 \pm 0.5\%$ ). At WS, the solar radiation ( $635.8 \pm 46.9 \text{ Wm}^{-2}$ ) was much higher  
30 than that at TC ( $563.5 \pm 46.1 \text{ Wm}^{-2}$ ,  $p < 0.01$ ), while the average wind speed at TC ( $4.6 \pm 0.1 \text{ ms}^{-1}$ )

1 was significantly lower than that measured at WS ( $7.2 \pm 0.2 \text{ms}^{-1}$ ). The lower wind speed at TC  
 2 was related to the roughness of underlying surfaces. However, no statistical differences were  
 3 found for the average wind direction (about  $81^\circ$ , northeast wind) at the two sites, indicating that  
 4 the two sites were probably under the influence of similar air masses in most cases.

5 The NO, NO<sub>2</sub>, CO, SO<sub>2</sub> and total VOCs (the sum of NMHCs and carbonyls) had lower average  
 6 and maximum mixing ratios at WS than those at TC. The lower levels of primary air pollutants at  
 7 WS were likely the results of fewer local emission sources, faster photochemical consumption  
 8 (as discussed later) and/or more favorable dispersion conditions (*e.g.*, higher wind speed). In  
 9 contrast, O<sub>3</sub> was much higher at WS (Table 1), attributable to the enhancements by both  
 10 meteorological and photochemical effects, as discussed in sections 3.2 and 3.3.

11 **Table 1.** Descriptive statistics of meteorological parameters and trace gases at the two sites  
 12 during the sampling period.

Parameter	WS		TC	
	<i>Mean ± 95% C.I.</i>	<i>Max.</i>	<i>Mean ± 95% C.I.</i>	<i>Max.</i>
Temperature (°C)	25.7 ± 0.1	32.8	26.7 ± 0.1	35.4
Relative humidity (%)	82.8 ± 0.4	98.9	67.7 ± 0.5	96.8
Solar radiation (W m <sup>-2</sup> )*	635.8 ± 46.9	1026.8	563.5 ± 46.1	910.0
Wind speed (m s <sup>-1</sup> )	7.2 ± 0.2	23.8	4.6 ± 0.1	13.8
Wind direction (°)	81.3	-	80.9	-
O <sub>3</sub> (ppbv)	51.3 ± 1.2	173.0	30.0 ± 1.0	159.9
NO (ppbv)	0.7 ± 0.1	21.0	14.0 ± 0.8	115.7
NO <sub>2</sub> (ppbv)	4.3 ± 0.3	49.3	25.0 ± 0.6	104.2
CO (ppbv)	251.4 ± 6.5	727.7	560.5 ± 6.3	1047.9
SO <sub>2</sub> (ppbv)	2.4 ± 0.1	12.2	5.9 ± 0.1	19.1
NMHCs (ppbv)	12.7 ± 1.1	32.9	17.7 ± 1.7	60.0

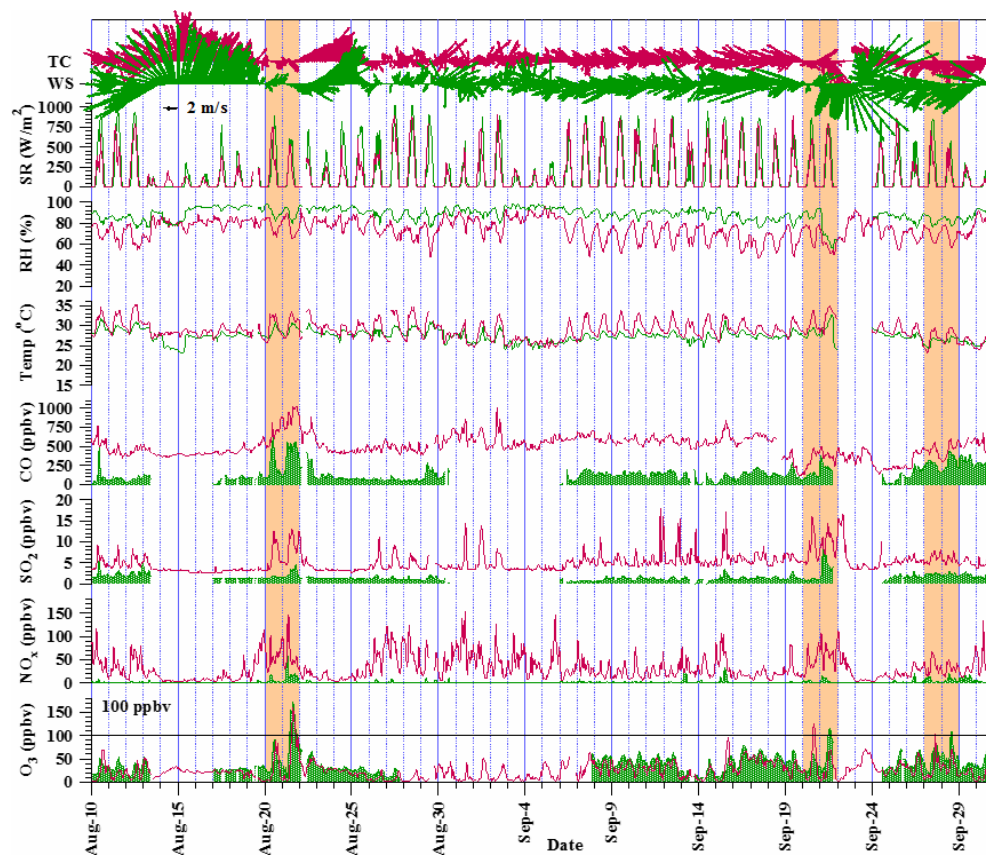
Carbonyls (ppbv)	7.9±0.7	16.3	9.2±0.7	26.5
------------------	---------	------	---------	------

---

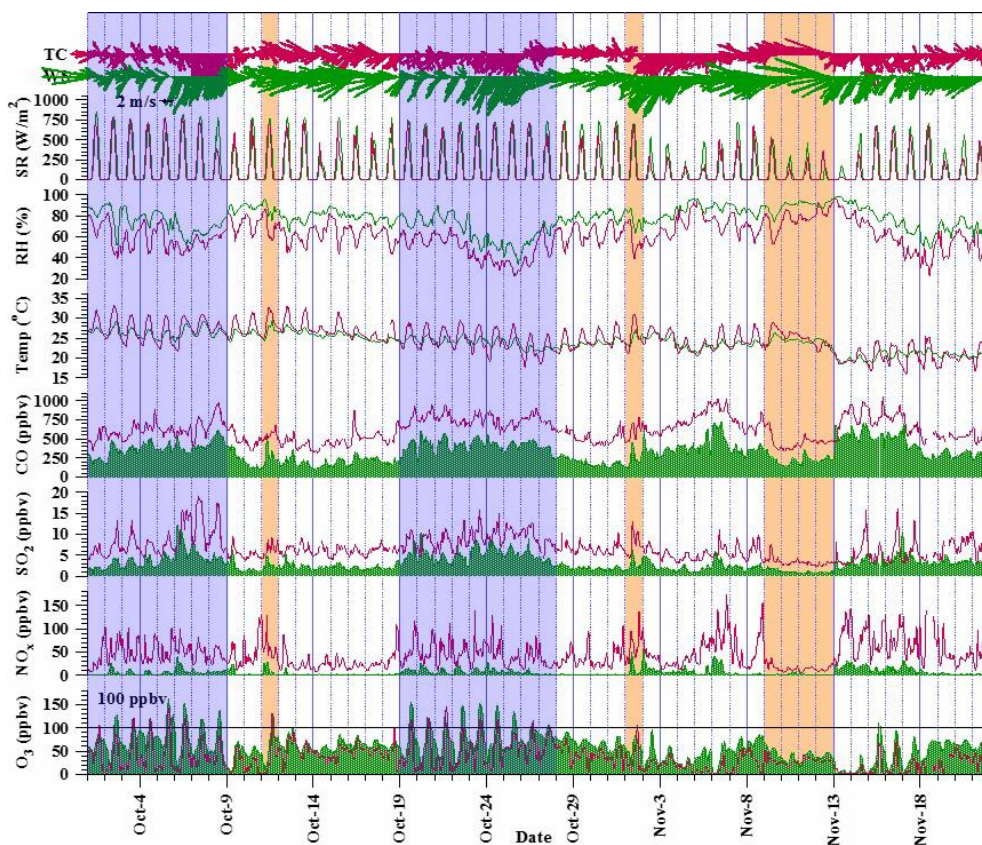
\* Average of the daily maximum solar radiation. *C.I.* denotes confidence interval.

Time series of local meteorological parameters and hourly mixing ratios of air pollutants at the two sites are illustrated in Figures 2a-2b. The temporal patterns of wind directions were generally similar at both sites, with the dominance of the southerly winds in August and northeastern winds between September and November. Occasionally, the northwesterly winds from the PRD region were observed.

This sampling campaign witnessed 17 O<sub>3</sub> episodes and 7 near-O<sub>3</sub> episode days at TC, which refers to the days with maximum hourly mixing ratio of O<sub>3</sub> higher than 100 ppbv and within the range of 80-100 ppbv, respectively. (80 ppbv was Level I of China National Ambient Air Quality Standard for O<sub>3</sub>). At WS, 21 O<sub>3</sub> episodes and 6 near-O<sub>3</sub> episodes were recorded. Specifically, 13 O<sub>3</sub> episode days were simultaneously observed at the two sites, with the rest occurred exclusively at one site. On one hand, the primary air pollutants (CO, SO<sub>2</sub> and NO<sub>x</sub>) generally increased during O<sub>3</sub> episodes, implying enhanced O<sub>3</sub> formation potentials from the precursors. On the other hand, O<sub>3</sub> episodes were always accompanied by the synoptic conditions, *i.e.*, tropical cyclone (typhoon in the mature form) and continental anticyclone, and/or mesoscale circulations such as SLB, as detailed in Table S4. For example, the two multi-day O<sub>3</sub> episode events, *i.e.*, 1-8 Oct. and 19-27 Oct. (highlighted in blue in Figure 2), were strongly associated with continental high pressure. These episode days generally had high temperature, northerly winds, and intensive solar radiation, with air flows largely from the inland or the coastal areas. Also, the mixing ratios of CO, NO<sub>2</sub> and SO<sub>2</sub> usually increased during these days, suggesting the accumulation of local air pollutants and/or the increasing contribution from regional transport. In contrast, O<sub>3</sub> episodes under the influence of tropical cyclones (highlighted in orange in Figure 2) featured high temperature, strong solar radiation and typically calm or moderate northwesterly to northeasterly winds, except for typhoon “Haiyan” occurred on 9-12 Nov. (discussed in section 3.2.1). These conditions were all conducive to the formation and accumulation of O<sub>3</sub>. Additionally, SLB was also an important factor regulating O<sub>3</sub> pollution in this region during O<sub>3</sub> episodes (Table S4). Detailed discussions can be found in section 3.2.3.



1  
 2 **Figure 2a.** Time series of trace gases and meteorological parameters observed for the sampling  
 3 period of 10 Aug. - 30 Sept. at WS (green) and TC (red). The black line of 100 ppbv is the  
 4 threshold for O<sub>3</sub> episode definition. The dates seriously affected by continental high pressure and  
 5 tropical cyclones are shaded in blue and orange, respectively. Note that there are some data  
 6 missing in these months due to extremely bad weather conditions and instrumental failure.  
 7



1  
 2 **Figure 2b.** Time series of trace gases and meteorological parameters observed for the sampling  
 3 period of 1 Oct. - 21 Nov at WS (green) and TC (red). The black line of 100 ppbv is the  
 4 threshold for O<sub>3</sub> episode definition. The dates seriously affected by continental high pressure  
 5 and tropical cyclones are shaded in red and orange, respectively.

6  
 7 **3.2 Meteorological influence on O<sub>3</sub> mixing ratios**

8 Descriptive statistics of meteorological parameters during O<sub>3</sub> episode and non-episode days are  
 9 summarized in Table 2. On episode days the wind speed and relative humidity were lower  
 10 whereas solar radiation was stronger at both sites, suggesting that this type of weather condition  
 11 was conducive to the formation and accumulation of tropospheric O<sub>3</sub>. Furthermore, the wind  
 12 direction during non-episodes was predominantly from the east (SCS), while on episodes the  
 13 winds mainly came from the north and northeast which might bring more pollutants from the  
 14 urban areas of Hong Kong and inland PRD to the sampling sites. The characteristics of O<sub>3</sub>  
 15 pollution under different weather conditions were discussed below.

1  
 2 **Table 2.** Descriptive statistics (Mean±95% C.I.) of meteorological parameters at the two sites  
 3 during O<sub>3</sub> episodes and non-O<sub>3</sub> episodes days.

Parameter	WS		TC	
	<i>O<sub>3</sub> episode</i>	<i>Non-O<sub>3</sub> episode</i>	<i>O<sub>3</sub> episode</i>	<i>Non-O<sub>3</sub> episode</i>
<b>Temperature (°C)</b>	25.3±0.2	25.8±0.1	26.3±0.3	26.8±0.2
<b>Wind speed (m s<sup>-1</sup>)</b>	5.3±0.2	7.7±0.2	3.7±0.2	4.8±0.1
<b>Wind direction (°)</b>	45.1	89.1	19.5	86.8
<b>Relative humidity (%)</b>	71.7±1.2	85.7±0.4	58.4±1.4	69.6±0.6
<b>Solar radiation (W m<sup>-2</sup>)*</b>	723.2±26.1	613.7±57.6	699.0±29.1	537.0±53.1

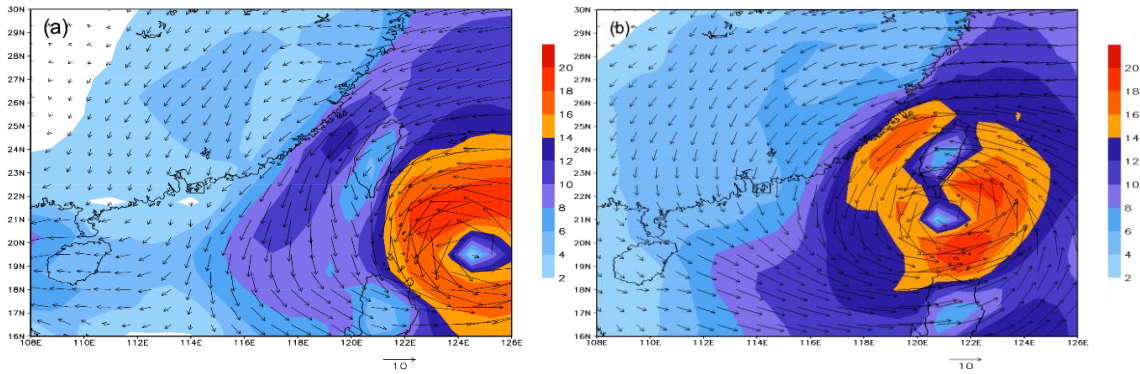
4 \* Average of the daily maximum solar radiation. *C.I.* denotes confidence interval.

5  
 6 *3.2.1 Tropical cyclones*  
 7 Tropical cyclone (low-pressure system) is one of the main meteorological conditions conducive  
 8 to the occurrence of O<sub>3</sub> episodes in Hong Kong (Yin, 2004; Ling et al., 2013). In this study, 7  
 9 episode days and 3 near-episode days were closely associated with 5 tropical cyclones (*i.e.*,  
 10 Trami, Usagi, Wutip, Nari and Krosa) (Table S4 and Figure S4). For example, Trami caused the  
 11 worst O<sub>3</sub> episode on 21 Aug. with the highest peak hourly O<sub>3</sub> mixing ratios of 160 and 173 ppbv  
 12 at TC and WS, respectively. These episode or near-episode days usually appeared 1-2 days  
 13 before the arrival of the tropical cyclones, because the large-scale peripheral subsidence of the  
 14 tropical cyclones usually creates the meteorological conditions favorable to the formation and  
 15 accumulation of O<sub>3</sub>, such as inversion layer, high temperature, low humidity, intensive light, and  
 16 weak winds (Wang et al., 1998; Yin, 2004). The tropical cyclones also cause anti-clockwise air  
 17 flows at their outskirts affecting the wind directions and subsequent the regional transport of air  
 18 pollution. Figure 3 illustrates surface wind fields and air movement two days (*i.e.*, 20-21 Sept.)  
 19 before the occurrence of Usagi as an example. It can be seen that when Usagi approached  
 20 southeastern area of Hong Kong, it led to weak northeasterly and later northwesterly winds  
 21 which potentially delivered O<sub>3</sub> and its precursors from highly polluted inland PRD region to the



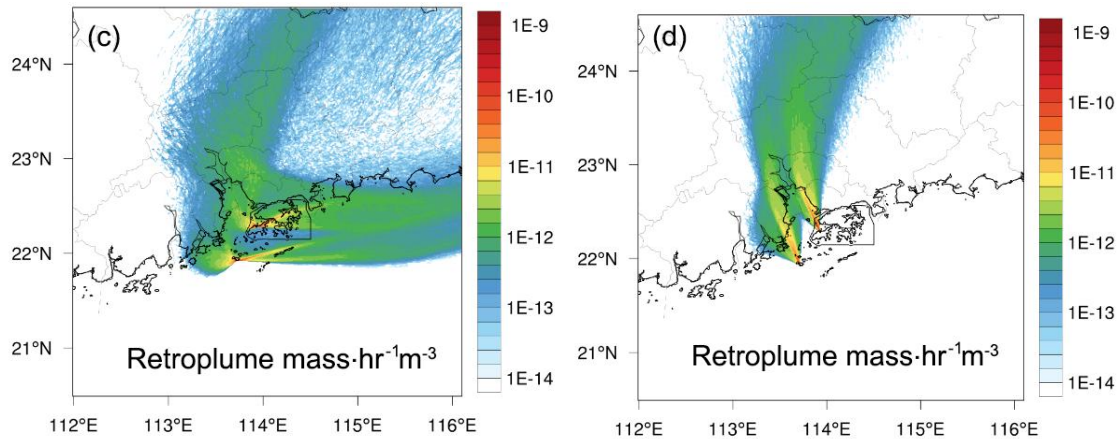
1 sampling sites (Yin, 2004; Wei et al., 2016; Wang et al., 2017a). The wind speed was lower than  
2  $4 \text{ m s}^{-1}$  at the sampling sites and in their surrounding area on 20 Sept. (Figure 3a), and it  
3 gradually increased on the next day (21 Sept.) with the approaching of the tropical cyclone  
4 (Figure 3b). It is noteworthy that the rarely occurred westerly and northwesterly winds caused  
5 tropical cyclones resulted in unsynchronized occurrence of  $\text{O}_3$  episodes between the two sites  
6 (Figures 3c & d). Namely, high  $\text{O}_3$  values were observed at TC only on 20 Sept., while  $\text{O}_3$  started  
7 to increase at WS on the next day (21 Sept.). This discrepancy might indicate the transport of  $\text{O}_3$   
8 and/or its precursors from terrestrial area to the offshore site driven by tropical cyclone.

9 Please note, not all tropical cyclones would cause high levels of  $\text{O}_3$ . For example, the tropical  
10 cyclone Haiyan observed on 9-12 Nov. over the SCS did not cause high  $\text{O}_3$  levels (Figure 2b).  
11 Because the origin of Haiyan was at a lower latitude (southern Guam) and it moved on the  
12 waters southwest of PRD (Figure S4), the anti-clockwise air flow caused easterly and  
13 southeasterly winds in the north and northeast outer band of Haiyan. The winds originated from  
14 SCS brought in clean marine air to the sampling sites, resulting in dilution and dispersion of  
15 local air pollutants.



16





1  
 2 **Figure 3.** Model simulated 10 m wind vectors (arrows) and wind speed (shaded, unit:  $\text{m s}^{-1}$ ), and  
 3 the distribution of air mass concentrations (unit:  $\text{mass hr}^{-1} \text{m}^{-3}$ ) within surface 100 m simulated  
 4 by HYSPLIT Lagrangian backward particle release model with WS and TC as the starting points  
 5 two days (20 Sept. 2013) before (a, c) and one day (21 Sept. 2013) before (b, d) the arrival of  
 6 Usagi.

7

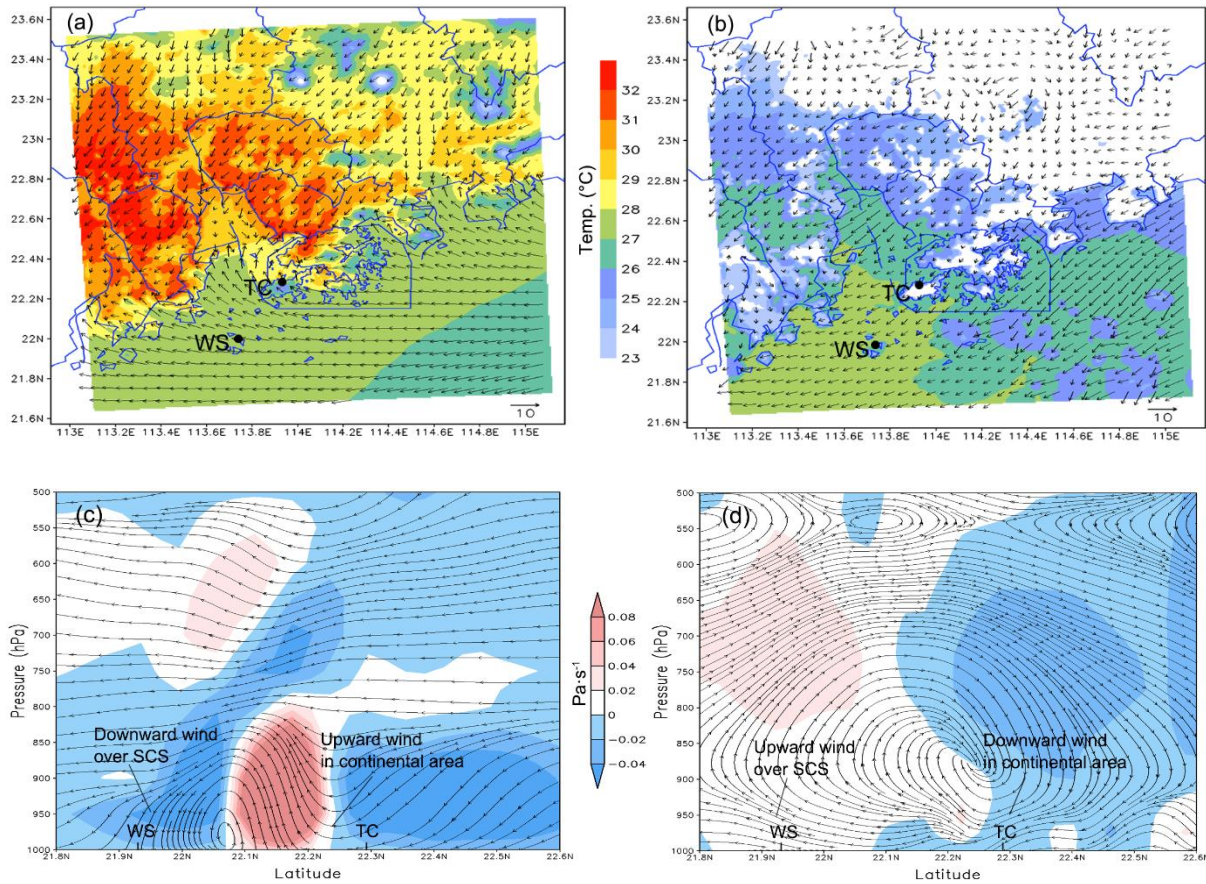
### 8 3.2.2 Continental anticyclones

9 In addition to tropical cyclones, the continental anticyclone (high-pressure system) was  
 10 frequently observed in the region, which often caused high  $\text{O}_3$  concentrations. For example, two  
 11 multi-day  $\text{O}_3$  episodes (1-8 Oct. and 19-27 Oct.) occurred at the sampling sites when there were  
 12 intensive continental anticyclones and weak Western Pacific Subtropical High (WPSH) to the  
 13 north of Hong Kong (see Figure S5 as examples). The SLBs also occurred occasionally during  
 14 the first several days of the two continental high pressure systems when the synoptic winds were  
 15 relatively weak (*i.e.*, 2-5 Oct. and 19-21 Oct.). The clockwise and slow movement of the air  
 16 masses caused northeasterly and easterly winds to the sampling sites and brought in densely  
 17 polluted air from the inland (Figure 2b) to the coastal areas of the SCS. For example, the CO  
 18 mixing ratios were significantly elevated during these episode days, with an average of 409 and  
 19 683 ppbv at WS and TC, respectively, which were higher than other episode days. The  
 20 continuous input of exotic air pollutants provided essential “fuel” to local photochemical  
 21 production of  $\text{O}_3$ , leading to the severe multi-day  $\text{O}_3$  episodes.

### 1 3.2.3 Sea-land breeze (SLB) circulation

2 During the sampling period, SLB circulations in the study area were identified on 21 out of 104  
3 sampling days. The occurrence frequency was comparable to that reported by Zhang and Zhang  
4 (1997) who discovered 70 SLB days in a year in the same region. In this study, 12 O<sub>3</sub> episode  
5 days were thought to be influenced by SLB (see Table S4), with 5 of them (27-28 Sept., 11-12  
6 Oct. and 1 Nov.) under the dominance of tropical cyclones (*i.e.*, Wutip, Nari and Krosa) and the  
7 other 7 days in association with the continental anticyclones. In addition to the effects of tropical  
8 cyclones and continental anticyclones discussed above, SLB also posed non-negligible impact on  
9 O<sub>3</sub> pollution in these cases.

10 SLB circulation is driven by sea-land thermal difference and topographic conditions, and usually  
11 happens when the synoptic winds are weak (Liu et al., 2002; Lo et al., 2006; Lu et al., 2009b).  
12 On a typical SLB day, wind blows onshore during the day (sea breeze) and offshore in the  
13 evening (land breeze). However, the transition time of breezes in this study was found to vary in  
14 a wide range. The sea breeze switched to land breeze between 00:00 and 08:00 with a median of  
15 03:00 for breeze shifting, and 11:00 – 18:00 with the median of 14:00 was the time when land  
16 breeze turned to sea breeze. Ding et al. (2004) also reported this phenomenon and pointed out  
17 that the start time of sea breezes in Hong Kong was generally delayed to noontime due to the  
18 synoptic northerly winds blowing from the continental areas to SCS, particularly on O<sub>3</sub> episode  
19 days when northerly winds dominated in Hong Kong. For example, the sea breeze commenced at  
20 15:00 on 3 Oct. and transited to land breeze at 4:00 on 4 Oct. (Figure 4). Figures 4a and 4b  
21 depict the surface wind fields with a sea breeze and a land breeze, respectively. The vertical wind  
22 fields with the sea breeze and land breeze are presented in Figures 4c and 4d, respectively.  
23 Surface and vertical SLB circulations were clearly seen in these panels of Figure 4. The  
24 mesoscale circulations caused by SLB might promote the interactions between the continental  
25 (TC) and marine (WS) atmospheres. Specifically, the primary air pollutants observed at TC  
26 could be transported to WS by land breeze. Moreover, the air masses could return to TC after  
27 sufficient photochemical evolutions over SCS, during which O<sub>3</sub> might also be elevated in the  
28 continental areas.



1  
 2  
 3 **Figure 4.** SLB circulation on 3-4 Oct. 2013, showing surface wind pattern (arrows) and  
 4 temperature (color) at 17:00 on 3 Oct. (a) and at 04:00 on 4 Oct. (b). Vertical cross-section  
 5 (taken over a longitude of 113.85 °E, mean of the longitudes of TC and WS) depicting the v-w  
 6 wind stream (arrow) and the index of  $\omega * 100$  (color) at 17:00 on 3 Oct. (c); and at 04:00 on 4  
 7 Oct. (d). For figures (c) and (d), the blue color (negative) and light red color (positive) present  
 8 downward and upward winds, respectively. Figures (a) and (c) represent a sea breeze, and  
 9 Figures (b) and (d) show a land breeze. Note that  $\omega$  is the vertical velocity in isobaric  
 10 coordinates.

### 12 3.3 Chemical characteristics of air masses

#### 13 3.3.1 Chemical composition

14 To inspect the chemical characteristics of air masses on O<sub>3</sub> episode days and non-O<sub>3</sub> episode  
 15 days, chemical species are statistically summarized at the two sites (Table 3). As expected, the

1 levels of all pollutants (*i.e.*, O<sub>3</sub>, NO<sub>2</sub>, CO, SO<sub>2</sub>, NMHCs and carbonyls) were significantly higher  
2 on O<sub>3</sub> episode days for both sites ( $p<0.05$ ), except for the comparable or even lower NO due to  
3 its titration to O<sub>3</sub> (see Section 3.3.2). Table S5 shows statistics of the top 10 NMHC and the top 3  
4 carbonyl species observed during O<sub>3</sub> episodes and non-episodes at the two sites. The dominant  
5 species were quite similar regardless of episode or non-episode days at both sites. The higher  
6 concentrations of both primary and secondary pollutants on episode days than those on non-  
7 episode days were likely due to more intense photochemical reactions, more local pollutant  
8 accumulation as well as the regional transport of more highly polluted air masses. On the other  
9 hand, the similar NMHCs composition at both sites during both episodes and non-episodes  
10 indicated somewhat interaction of air masses between the two sites regardless of O<sub>3</sub> levels.

11 It is worth to mention that O<sub>3</sub> was much higher at WS than that at TC during both episodes and  
12 non-episodes ( $p<0.01$ ), with an average difference of 30.2 ppbv and 16.7 ppbv, respectively  
13 (Table 3), though the levels of O<sub>3</sub> precursors (*i.e.*, NO<sub>x</sub> and VOCs) at WS were lower. Insight  
14 into VOC ratios found that ethene/ethane ( $0.5\pm0.04$ ) and toluene/benzene ( $2.2\pm0.5$ ) at WS were  
15 significantly ( $p<0.05$ ) lower than those at TC ( $0.7\pm0.1$  and  $2.9\pm0.4$ , respectively), likely  
16 indicating that the air masses at WS were more aged (Guo et al., 2007). Therefore, the higher O<sub>3</sub>  
17 at WS might be partially attributable to the aging of air masses (*e.g.*, during the transport of  
18 continental air).

1 **Table 3.** Descriptive statistics (Mean $\pm$ 95% *C.I.*) of measured air pollutants, simulated OH,  
 2 HO<sub>2</sub> and RO<sub>2</sub> at the two sites during O<sub>3</sub> episodes and non-O<sub>3</sub> episodes days.

Parameter	WS		TC	
	<i>O<sub>3</sub> episode</i>	<i>Non-O<sub>3</sub> episode</i>	<i>O<sub>3</sub> episode</i>	<i>Non-O<sub>3</sub> episode</i>
O <sub>3</sub> (ppbv)	74.3 $\pm$ 3.0	43.9 $\pm$ 1.0	44.1 $\pm$ 3.6	27.2 $\pm$ 0.8
O <sub>x</sub> (ppbv)	81.6 $\pm$ 2.9	47.8 $\pm$ 1.0	83.3 $\pm$ 3.7	49.4 $\pm$ 1.0
NO (ppbv)	0.9 $\pm$ 0.2	0.5 $\pm$ 0.2	11.5 $\pm$ 1.4	14.5 $\pm$ 0.9
NO <sub>2</sub> (ppbv)	8.5 $\pm$ 0.9	2.0 $\pm$ 0.5	39.2 $\pm$ 1.7	22.2 $\pm$ 0.6
CO (ppbv)	391.4 $\pm$ 9.1	209.4 $\pm$ 6.8	652.9 $\pm$ 16.0	541.9 $\pm$ 6.5
SO <sub>2</sub> (ppbv)	4.3 $\pm$ 0.2	1.9 $\pm$ 0.1	8.1 $\pm$ 0.3	5.5 $\pm$ 0.1
NMHCs (ppbv)	17.7 $\pm$ 1.4	9.6 $\pm$ 1.2	20.2 $\pm$ 2.2	16.8 $\pm$ 2.1
Carbonyls (ppbv)	10.3 $\pm$ 0.8	5.4 $\pm$ 0.4	12.0 $\pm$ 1.3	8.1 $\pm$ 0.7
NO <sub>2</sub> /NO (ppbv/ppbv)	12.7 $\pm$ 1.1	4.7 $\pm$ 0.5	3.4 $\pm$ 0.4	1.5 $\pm$ 0.2
Simulated OH ( $\times 10^6$ molecules cm <sup>-3</sup> )	5.5 $\pm$ 0.9	4.4 $\pm$ 0.6	1.5 $\pm$ 0.4	2.1 $\pm$ 0.3
Simulated HO <sub>2</sub> ( $\times 10^7$ molecules cm <sup>-3</sup> )	29 $\pm$ 4.9	45 $\pm$ 4.2	2.0 $\pm$ 1.0	2.6 $\pm$ 0.7
Simulated RO <sub>2</sub> ( $\times 10^7$ molecules cm <sup>-3</sup> )	19 $\pm$ 3.8	47 $\pm$ 6.2	1.2 $\pm$ 0.6	1.4 $\pm$ 0.4

3 \* Average of the daily maximum solar radiation. *C.I.* denotes confidence interval. O<sub>x</sub> = O<sub>3</sub> + NO<sub>2</sub>.

### 5 3.3.2 Influence of NO titration

6 Apart from the age of air masses, NO titration is another important factor influencing O<sub>3</sub>  
 7 concentration. In areas with high NO levels, the NO titration (O<sub>3</sub> + NO  $\rightarrow$  NO<sub>2</sub> + O<sub>2</sub>) is a  
 8 main process consuming O<sub>3</sub>. In this study, the average NO mixing ratio at TC was 14.0 $\pm$ 0.8  
 9 ppbv, compared to 0.7 $\pm$ 0.1 ppbv at WS (Table 1). The much lower NO at WS implied  
 10 weaker titration to O<sub>3</sub>, which enabled the survival of more O<sub>3</sub> and caused substantial residual  
 11 O<sub>3</sub> at WS particularly at night time when there were no photochemical reactions (Figure 2  
 12 and Figure S6). Another direct evidence of NO titration effect was the trough of O<sub>3</sub> during  
 13 the morning rush hours (06:00-07:00), together with an increase of NO<sub>2</sub> (Figure S6).

1 Furthermore, the total oxidants ( $O_x = O_3 + NO_2$ ), which are usually adopted to take into  
2 account the NO titration influence, were comparable ( $p > 0.05$ ) between TC and WS with  
3 mean values of  $83.3 \pm 3.7$  ppbv and  $81.6 \pm 2.9$  ppbv during  $O_3$  episodes, and  $49.4 \pm 1.0$  ppbv and  
4  $47.8 \pm 1.0$  ppbv during non-episodes, respectively (Table 3). This was reasonable in view of  
5 the interactions between the two sites. However, the remarkably higher  $O_3$  and lower NO at  
6 WS indicated that NO titration was a determinant factor regulating the  $O_3$  levels at both sites.

7 Moreover, NO titration is generally more significant on high  $O_3$  days, resulting in higher  
8  $NO_2/NO$  ratios due to the conversion of NO to  $NO_2$  by  $O_3$ . Indeed, the mean  $NO_2/NO$  ratios  
9 increased from  $4.7 \pm 0.5$  at WS and  $1.5 \pm 0.2$  at TC during non-episodes to  $12.7 \pm 1.1$  and  
10  $3.4 \pm 0.4$  during  $O_3$  episodes, respectively, implying that more  $O_3$  was titrated by NO during  
11 episodes. As a result, NO at TC was lower ( $p < 0.01$ ) during  $O_3$  episodes than during non-  
12 episodes (Table 3). It is noteworthy that NO at WS was on the same level between  $O_3$  episode  
13 and non- $O_3$  episode days ( $p > 0.05$ ). This probably related to the weak titration at this marine  
14 site due to the trivial NO concentrations in both periods, as well as the counteracting effect of  
15 the increased transport of NO under northerly winds against the enhanced titration during  $O_3$   
16 episodes.

17 The aforementioned discussion demonstrated that NO titration played an important role in  
18 altering  $O_3$  distribution, especially on  $O_3$  episodes days. The lower NO (weaker NO titration)  
19 partially resulted in the higher  $O_3$  concentrations observed at WS.

### 20 *3.3.3 Atmospheric oxidative capacity and $O_3$ production rate*

21  $O_3$  formation is driven by the transformation and recycling of oxidative radicals, including  
22 OH,  $HO_2$  and  $RO_2$ , collectively referred to as  $RO_x$  hereafter. The production and loss rates of  
23 these radicals, and their equilibrium concentrations on the canister sampling days were  
24 simulated by the PBM-MCM model, as shown in Figure S7. We noticed that WS featured  
25 significantly higher levels of these oxidative radicals on average ( $p < 0.05$ ). The daytime  
26 (7:00-19:00 LT) average OH concentration at TC and WS was  $(1.5 \pm 0.4) \times 10^6$  molecules  $cm^{-3}$   
27 and  $(5.5 \pm 0.9) \times 10^6$  molecules  $cm^{-3}$  during  $O_3$  episodes, respectively. Consistently,  $HO_2$  and  
28  $RO_2$  at WS were well above those at TC (Table 3). This pattern was also applicable between  
29 the two sites during non-episodes. Furthermore, while the difference in OH concentration  
30 became less on non-episode days, the gaps for peroxy radicals ( $HO_2$  and  $RO_2$ ) between TC  
31 and WS widened, as listed in Table 3. From non-episodes to episodes, OH increased at WS  
32 alongside with the decreases of  $HO_2$  and  $RO_2$ , likely indicating more conversion of  $HO_2$  to

1 OH by NO, which is an important pathway leading to O<sub>3</sub> formation. Details about this were  
2 shown later.

3 To explain the inter-site differences of the concentrations of oxidative radicals and the  
4 variations between O<sub>3</sub> episodes and non-episodes, Figure S7 also provides the breakdowns of  
5 the production and loss rates of OH, HO<sub>2</sub> and RO<sub>2</sub> at TC and WS, separately. Overall, the  
6 reaction between HO<sub>2</sub> and NO dominated the production of OH at both sites, with the  
7 contribution of 69.4±2.0% and 81.0±1.5% at TC and WS, respectively. While the photolysis  
8 of HONO ranked the second in the production of OH at TC (22.2±2.1%), the contribution of  
9 this pathway to OH production at WS (3.7±0.6%) was overstepped by O<sub>3</sub> photolysis  
10 (13.1±1.6%). This discrepancy was associated with the higher HONO and lower O<sub>3</sub> at TC  
11 (Figure S1 and Table 3). As expected, the production rate of OH through HO<sub>2</sub> reacting with  
12 NO experienced the most significant increase from 1.4±0.2×10<sup>7</sup> molecules cm<sup>-3</sup> s<sup>-1</sup> during  
13 non-episodes to 3.6±0.6×10<sup>7</sup> molecules cm<sup>-3</sup> s<sup>-1</sup> during O<sub>3</sub> episodes at WS, which explained  
14 more than 90% of the increase of the total OH production. In terms of the losses of OH,  
15 reaction between OH and NO<sub>2</sub> was the largest sink of OH at TC. However, OH-initiated  
16 oxidations of VOCs consumed most (52.7±1.8%) of OH at WS. This was reasonable in view  
17 of the much more abundant NO<sub>2</sub> at TC than at WS, in contrast to the smaller difference in  
18 NMHCs between the two sites (Table 3). Since OH can generally be recycled from the  
19 oxidation of VOCs, the lower OH at TC was likely caused by the lower O<sub>3</sub> photolysis and  
20 higher consumption of OH by NO<sub>2</sub>, despite the more intensive HONO photolysis. The overall  
21 oxidation rate of VOCs by OH was employed to indicate the atmospheric oxidative capacity  
22 in previous studies (Elshorbany et al., 2009; Xue et al., 2016). In this study, we found that the  
23 oxidation rate of VOCs at TC (6.1±2.1×10<sup>6</sup> molecules cm<sup>-3</sup> s<sup>-1</sup> during O<sub>3</sub> episodes and  
24 5.7±0.9×10<sup>6</sup> molecules cm<sup>-3</sup> s<sup>-1</sup> during non-episodes) was remarkably (*p*<0.05) lower than  
25 that at WS (O<sub>3</sub> episode: 15±2.5×10<sup>6</sup> molecules cm<sup>-3</sup> s<sup>-1</sup> and non-episode: 8.9±1.3×10<sup>6</sup>  
26 molecules cm<sup>-3</sup> s<sup>-1</sup>). The results revealed that the atmospheric oxidative capacity at TC was  
27 weaker than at WS for both O<sub>3</sub> episodes and non-episodes, inconsistent with the findings of  
28 Elshorbany et al. (2009) and Xue et al. (2016) who concluded that the atmospheric oxidative  
29 capacity was higher in more polluted environments due to the fact that the atmospheric  
30 oxidative capacity is positively proportional to the VOCs and OH levels. Both Elshorbany et  
31 al. (2009) and Xue et al. (2016) reported very high mixing ratios of VOCs (*e.g.* toluene of 9.5  
32 and 6.3 ppbv, respectively) in the polluted cases, which explained the strong atmospheric  
33 oxidative capacity. However, in this study, it is more likely that the higher NO<sub>x</sub> at TC

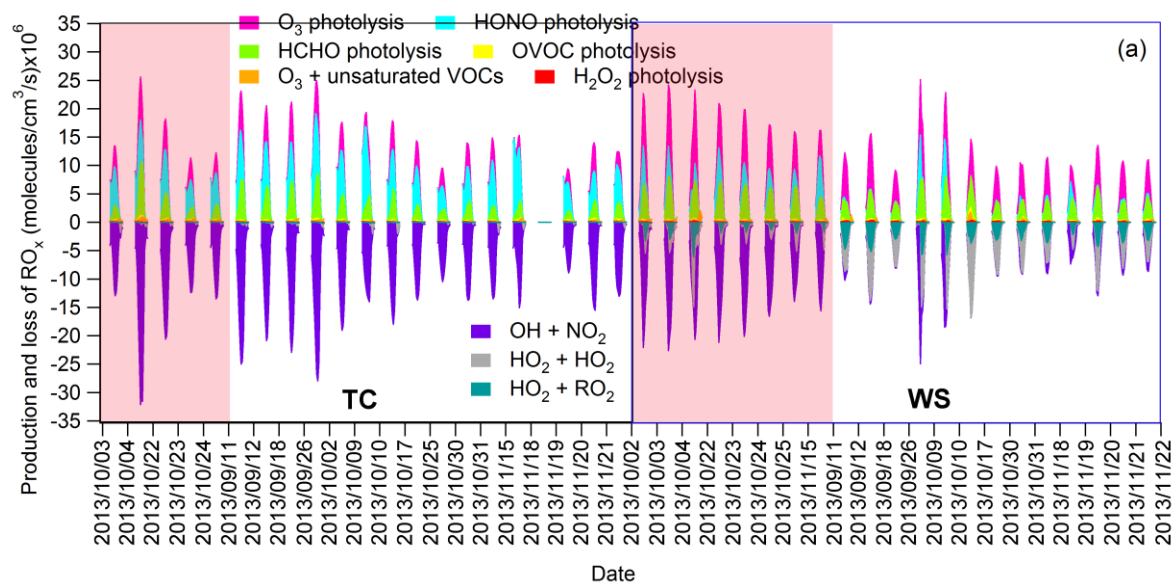
1 consumed more OH and resulted in lower oxidative capacity than at WS, despite the slightly  
2 higher VOCs at TC (Table 3).

3 For HO<sub>2</sub>, RO<sub>2</sub> reacting with NO accounted for 56.7±1.1% and 60.7±1.0% of HO<sub>2</sub> production  
4 at TC and WS, respectively. Oxidation of CO by OH was also an important pathway leading  
5 to HO<sub>2</sub> formation, second to RO<sub>2</sub>+NO at both sites. At TC, HO<sub>2</sub> was almost exclusively  
6 depleted by NO. However, 10.8±1.8% and 6.5±0.8% of the HO<sub>2</sub> losses were attributable to  
7 HO<sub>2</sub>-RO<sub>2</sub> and HO<sub>2</sub>-HO<sub>2</sub> reactions at WS, respectively, though HO<sub>2</sub>+NO was responsible for  
8 the most fraction (82.7±2.6%) of HO<sub>2</sub> losses. We believe that the more significant self-  
9 consumption of peroxy radicals at WS was closely related to the low NO<sub>x</sub> there, which  
10 hampered the transfer of oxygen atom from peroxy radicals to NO and further formation of  
11 O<sub>3</sub>. This was confirmed by the enhanced losses of HO<sub>2</sub> through reactions with HO<sub>2</sub> itself and  
12 RO<sub>2</sub> from 3.0±1.2% during O<sub>3</sub> episodes to 24.9±3.4% during non-episodes at WS, because  
13 NO<sub>x</sub> was more scarce during non-episodes at this site (Table 3). Similarly, in contrast to the  
14 negligible influence of RO<sub>2</sub> reacting with HO<sub>2</sub> on RO<sub>2</sub> budget at TC, HO<sub>2</sub>-RO<sub>2</sub> reactions  
15 played important role in losses of RO<sub>2</sub> at WS, particularly on non-episode days (Figure S7).  
16 When OH, HO<sub>2</sub> and RO<sub>2</sub> were summed up, the production and loss rate of RO<sub>x</sub> were obtained,  
17 as shown in Figure 5(a). Under such circumstance, the transformation and recycling pathways  
18 among these radicals can be neglected. For example, OH-initiated oxidation of VOCs  
19 consumes OH, which however generates RO<sub>2</sub>. Therefore, these reactions were not considered  
20 as sources or sinks of RO<sub>x</sub>. On one hand, HONO photolysis was the largest source of RO<sub>x</sub> at  
21 TC (53.7±2.6%), followed by the photolysis of HCHO (21.1±1.6%) and O<sub>3</sub> (18.7±1.5%).  
22 However, O<sub>3</sub> photolysis ranked the first among the sources of RO<sub>x</sub> at WS with the  
23 contribution of 38.6±2.3%, higher than the contributions from HCHO photolysis (34.3±1.4%)  
24 and HONO photolysis (18±2.5%). On the other hand, while the reaction between OH and  
25 NO<sub>2</sub> served as the sole sink of RO<sub>x</sub> at TC, it only explained 50% of RO<sub>x</sub> sink at WS with the  
26 other half attributable to self-consumption of peroxy radicals.

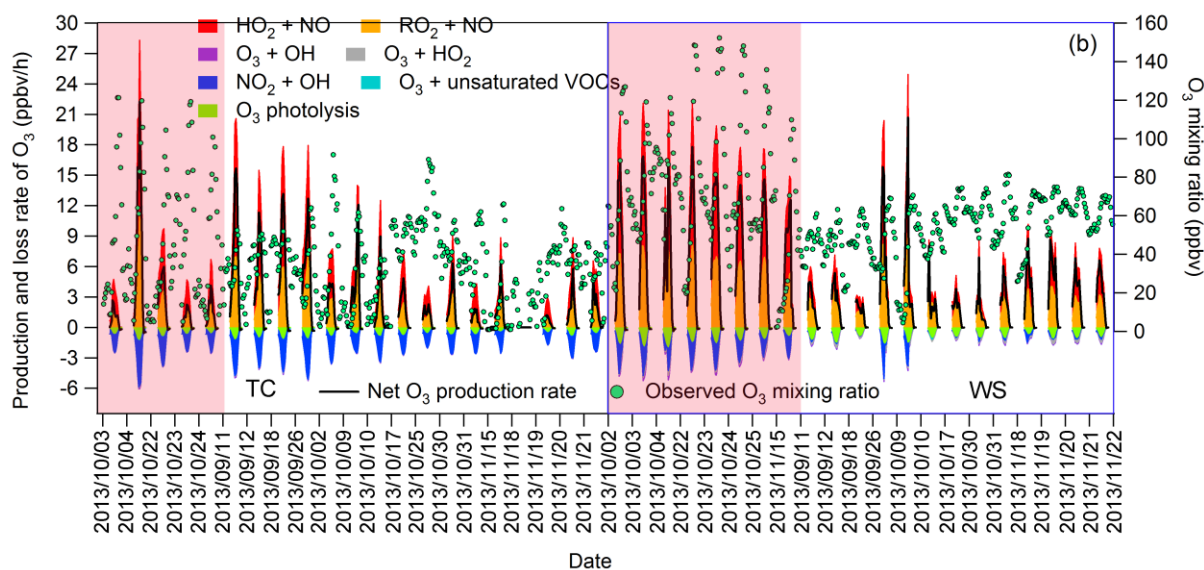
27 Furthermore, the production and loss rates of O<sub>3</sub> were simulated (Figure 5(b)). Despite the  
28 increased O<sub>3</sub> mixing ratio during episodes (Table 3), there was no significant change in net  
29 O<sub>3</sub> production between O<sub>3</sub> episodes (2.5±1.0 ppbv/h) and non-episodes (2.5±0.5 ppbv/h) at  
30 TC ( $p>0.05$ ), suggesting that regional transport might play critical roles in regulating O<sub>3</sub>  
31 levels at TC. In fact, previous studies (Huang et al., 2006; Jiang et al., 2008) have repeatedly  
32 confirmed that O<sub>3</sub> pollution at this site could be aggravated under northerly winds and/or



1 downdraft on the periphery of typhoon. In contrast, the net O<sub>3</sub> production increased  
 2 remarkably from non-episodes ( $2.8\pm 0.5$  ppbv/h) to O<sub>3</sub> episodes ( $6.6\pm 1.1$  ppbv/h) at WS.  
 3 Obviously, O<sub>3</sub> production at WS was much higher than at TC during O<sub>3</sub> episodes, while they  
 4 were comparable during non-episodes. This was likely due to the more abundant peroxy  
 5 radicals (RO<sub>2</sub> and HO<sub>2</sub>) at WS than at TC, in addition to the increased NO<sub>x</sub> during O<sub>3</sub>  
 6 episodes which enhanced the reactions between the peroxy radicals and NO (increasing O<sub>3</sub>  
 7 formation). Insight into the O<sub>3</sub> production pathways found that the reaction rates of RO<sub>2</sub>+NO  
 8 and HO<sub>2</sub>+NO were significantly enhanced from  $1.6\pm 0.2$  and  $2.0\pm 0.4$  ppbv/h during non-  
 9 episodes to  $3.2\pm 0.5$  and  $5.2\pm 0.9$  ppbv/h during O<sub>3</sub> episodes, respectively. Our recent study  
 10 (Wang et al., 2017b) revealed that O<sub>3</sub> formation at WS was in a transition regime and much  
 11 more sensitive to NO<sub>x</sub> during non-episodes, when O<sub>3</sub> production through peroxy radicals  
 12 reacting with NO was seriously limited by the low NO<sub>x</sub>. During O<sub>3</sub> episodes, with the  
 13 increase O<sub>3</sub> precursors (particularly NO<sub>x</sub>), these reactions were accelerated and the net O<sub>3</sub>  
 14 production increased substantially. Detailed discussion on the O<sub>3</sub> photochemistry at WS can  
 15 be found in our recent publication (Wang et al., 2017b).



16

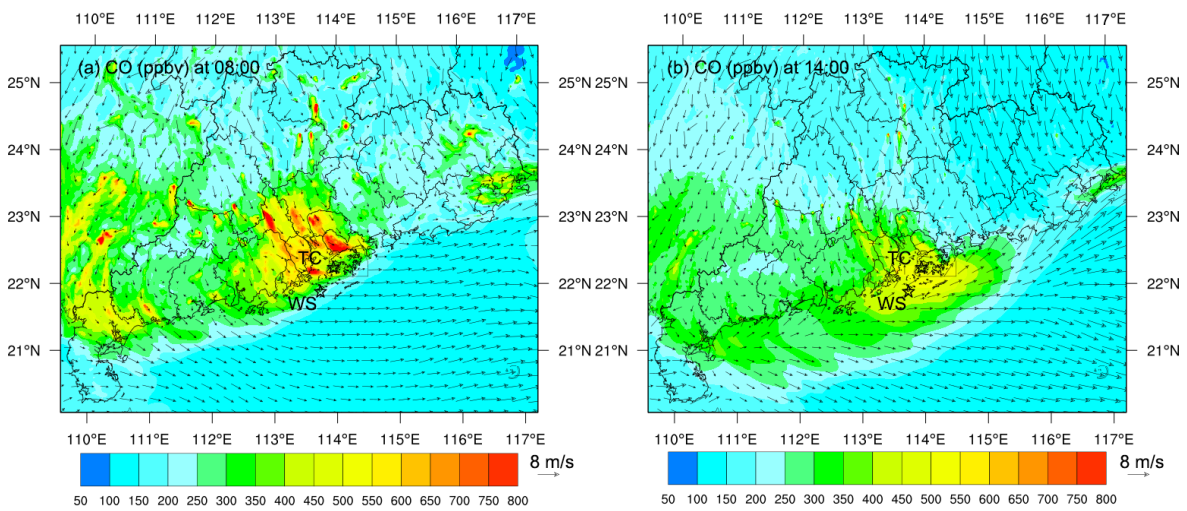


1  
 2 **Figure 5.** Daytime (7:00-19:00 LT) variations of the simulated production and loss rates of (a)  
 3 RO<sub>x</sub> and (b) O<sub>3</sub> at TC (left panel) and WS (right panel). O<sub>3</sub> episode days are highlighted in  
 4 red background. The dates are not consecutive due to the discontinuous canister sampling of  
 5 VOCs.

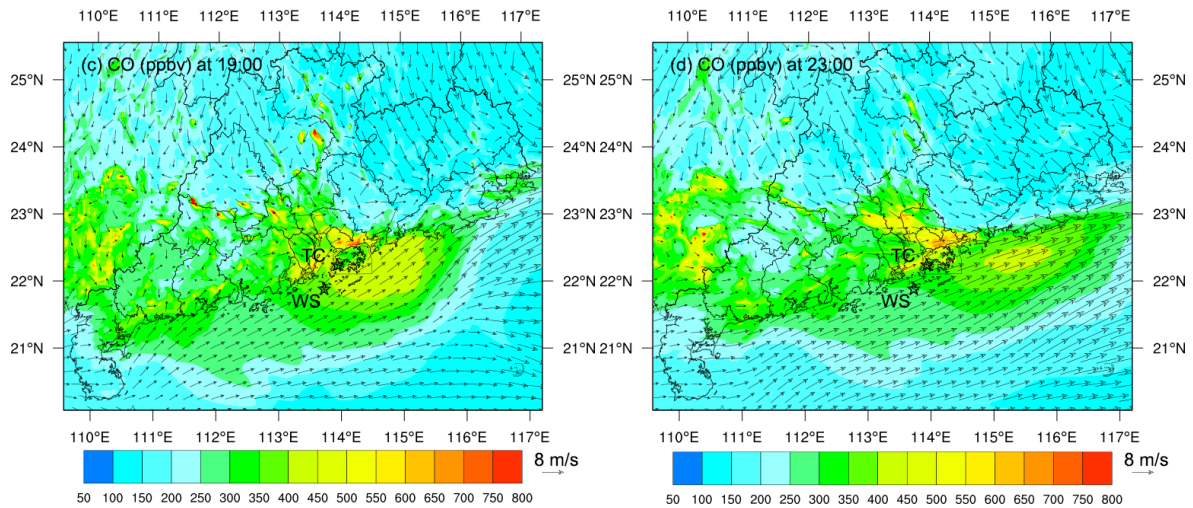
### 6 3.4 Impact of air mass interaction on O<sub>3</sub> pollution in coastal areas

7 Driven by various weather systems (*e.g.*, continental anticyclones, WPSH, tropical cyclones  
 8 and SLBs), continental and marine air masses frequently interact with each other in the  
 9 coastal areas. When continental air masses intrude into marine atmosphere, the chemical  
 10 composition and atmospheric oxidative capacity over the marine atmosphere will be altered  
 11 by the introduction of anthropogenic pollutants. Taken 21 Aug. as an example, when the  
 12 sampling sites (TC and WS) were under northwesterly to southwesterly winds caused by  
 13 tropical cyclone (Figure 2a), the maximum hourly O<sub>3</sub> reached 160 and 173 ppbv at TC and  
 14 WS, respectively. Correspondingly, the primary air pollutants all stayed on high levels,  
 15 compared to those during non-episodes (Figure 2a). Since WS was almost free of  
 16 anthropogenic emissions, the great abundances of both primary and secondary air pollutants  
 17 implied the influence of continental pollution on air quality at this site. Figures 6-7 depict the  
 18 spatial distributions of CO and O<sub>3</sub> over the region of interest at selective time (08:00, 14:00,  
 19 19:00 and 23:00) on 21 Aug., respectively. CO is presented as an example of primary air  
 20 pollutants emitted from anthropogenic sources. The spatiotemporal patterns of CO and O<sub>3</sub>  
 21 were simulated by WRF-CMAQ. Noticeably, the model well reproduced high level of CO in  
 22 PRD region at 08:00, which was reasonable in view of the vehicular emissions in urban areas

1 during morning rush hours. However, under the dominance of northwesterly winds in the  
 2 morning, the center of high CO moved to the coastal areas. Even though the winds changed  
 3 to southwesterly at noon, CO concentration over SCS was still remarkably elevated according  
 4 to the simulated results at 14:00. Further, the spatial distribution of CO at 19:00 and 23:00  
 5 confirmed the continuous movement of the polluted air masses away from the land under  
 6 southwesterly winds. It should be noted that the increase of CO in PRD region at 19:00 and  
 7 23:00 were most likely caused by the vehicle emissions during evening rush hours. Overall,  
 8 the dynamic distribution of CO in the study area clearly indicated the interaction between  
 9 continental and marine atmospheres. As a result of the intrusion of continental air, high level  
 10 of O<sub>3</sub> was simulated over SCS at 14:00 (Figure 7b), which was comparable to the observed  
 11 value (148 ppbv) at WS. Moreover, O<sub>3</sub> was even higher over SCS than that in continental  
 12 area, due mainly to the more aged air masses, lower NO titration and higher oxidative  
 13 capacity of the atmosphere (see section 3.3). Consistent with CO, the center of high O<sub>3</sub>  
 14 moved away from the land. At 19:00, the O<sub>3</sub>-laden air mass penetrated into the SCS ~300 km,  
 15 causing ~8,000 km<sup>2</sup> water area (8 times the area of Hong Kong) under high level of O<sub>3</sub> (>100  
 16 ppbv). This case provided solid evidence of the transport of continental air masses to SCS,  
 17 which aggravated air pollution (particularly O<sub>3</sub> pollution) in this offshore area.

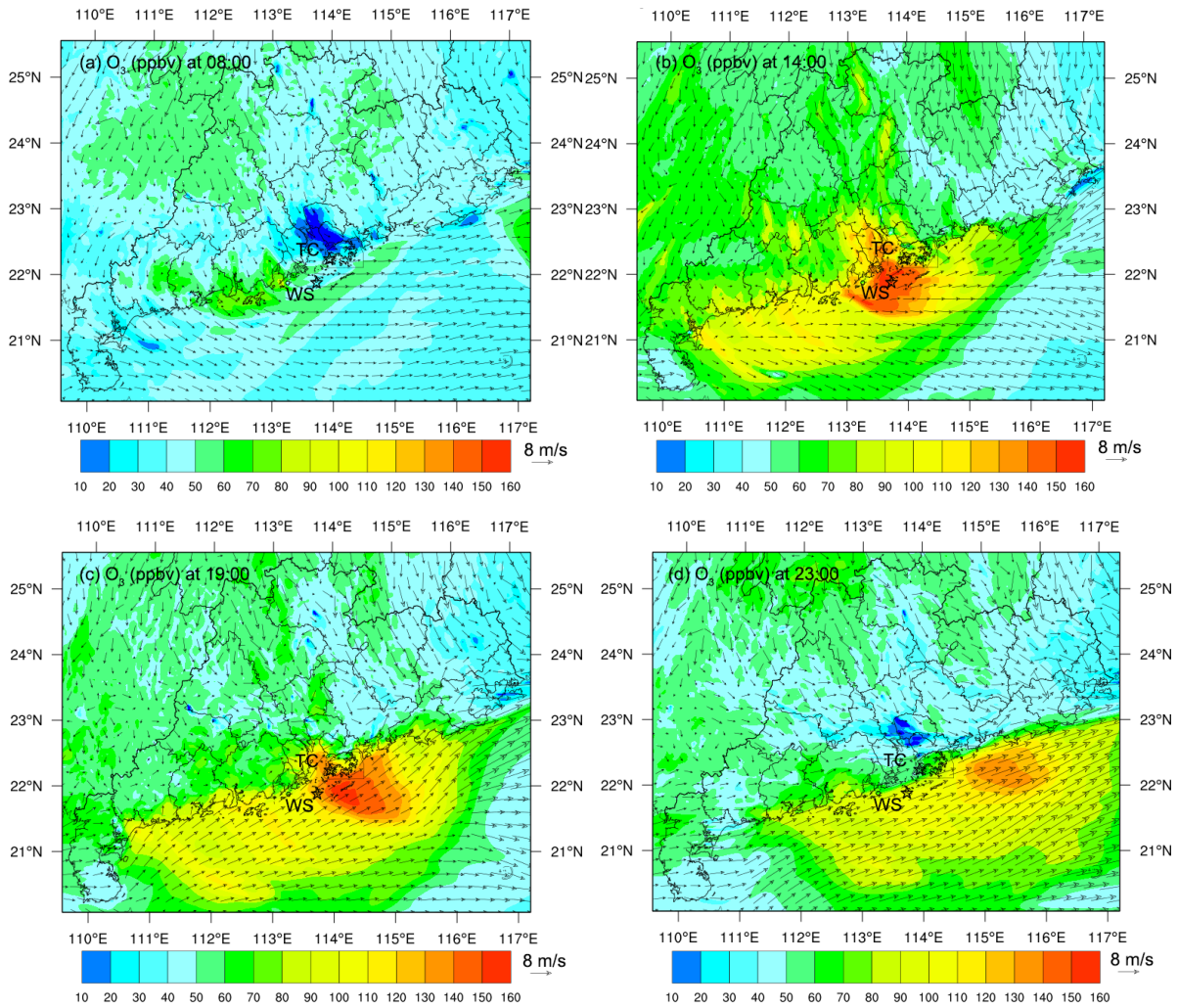


18



1

2 **Figure 6.** Spatial distribution of CO at 08:00 (a), 14:00 (b), 19:00 (c) and 23:00 (d) on 21  
 3 August simulated by WRF-CMAQ, taken as an example of the “Outflow” interaction pattern.  
 4 Arrows in the figure represent the surface wind field.



5

6 **Figure 7** Spatial distribution of O<sub>3</sub> at 08:00 (a), 14:00 (b), 19:00 (c) and 23:00 (d) on 21  
 7 August simulated by WRF-CMAQ, taken as an example of the “Outflow” interaction pattern.  
 8 Arrows in the figure represent the surface wind field.  
 9

1 In contrast to outflow of continental air masses, the continental area near the coast could also  
2 be immersed by oceanic air masses. The arrival of oceanic air masses generally brings  
3 substantial marine-originated compounds (e.g. dimethyl sulfide) to the continent and  
4 significantly alleviates the anthropogenic air pollution there. In fact, this is one of the main  
5 reasons for low O<sub>3</sub> mixing ratio observed in the PRD region in summertime when  
6 southwestern winds prevail (Wang et al., 2009; Wang et al., 2017a). In this study, it was also  
7 found that winds over the ocean increased the concentration of dimethyl sulfide at TC (Figure  
8 S8) and reduced the levels of almost all man-made air pollutants in many cases, mainly in  
9 summertime (Figure 2a).

10 In contrast, sea breezes carrying elevated O<sub>3</sub> formed over SCS might build up the terrestrial  
11 O<sub>3</sub> in the coastal area in some cases. Figure 8 shows the spatial distribution of O<sub>3</sub> over the  
12 study area on 3 Oct., as an example of SLB regulating O<sub>3</sub> formation and distribution (see  
13 Figure 4). Similar to the aforementioned scenario controlled by tropical cyclone, the  
14 simulated O<sub>3</sub> at 14:00 was generally higher over SCS than in the terrestrial area, indicating  
15 the transport of polluted air masses from the land to the sea area. This was confirmed by the  
16 prevailing northeasterly winds in the morning (08:00 here). However, the O<sub>3</sub>-laden air did not  
17 move far away from the land subsequently. Instead, it progressively approached the land,  
18 leading to increase of O<sub>3</sub> concentration in most parts of Hong Kong. This is because the wind  
19 direction in the coastal region changed from northeasterly to southeasterly at 17:00. Namely,  
20 the sea breeze appeared in late afternoon, which delivered the high O<sub>3</sub> formed over SCS to  
21 the continental areas near the coast. In fact, the air quality monitoring stations deployed in  
22 southern Hong Kong by HKEPD also recorded the O<sub>3</sub> peak in the evening when O<sub>3</sub> could not  
23 be formed locally (Figure S9), further confirming the recirculation of O<sub>3</sub>-laden air from SCS  
24 to coastal areas of Hong Kong under sea-breeze. However, the oceanic air did not penetrate  
25 further into the inland PRD, which was likely stopped by the strong northeasterly winds  
26 dominated in the inland areas. Overall, it can be seen that SLB as a common interaction  
27 between marine and continental atmospheres played important role in regulating O<sub>3</sub>  
28 formation and distribution in coastal region of SCS, which is also applicable to other similar  
29 mesoscale environments over the world.



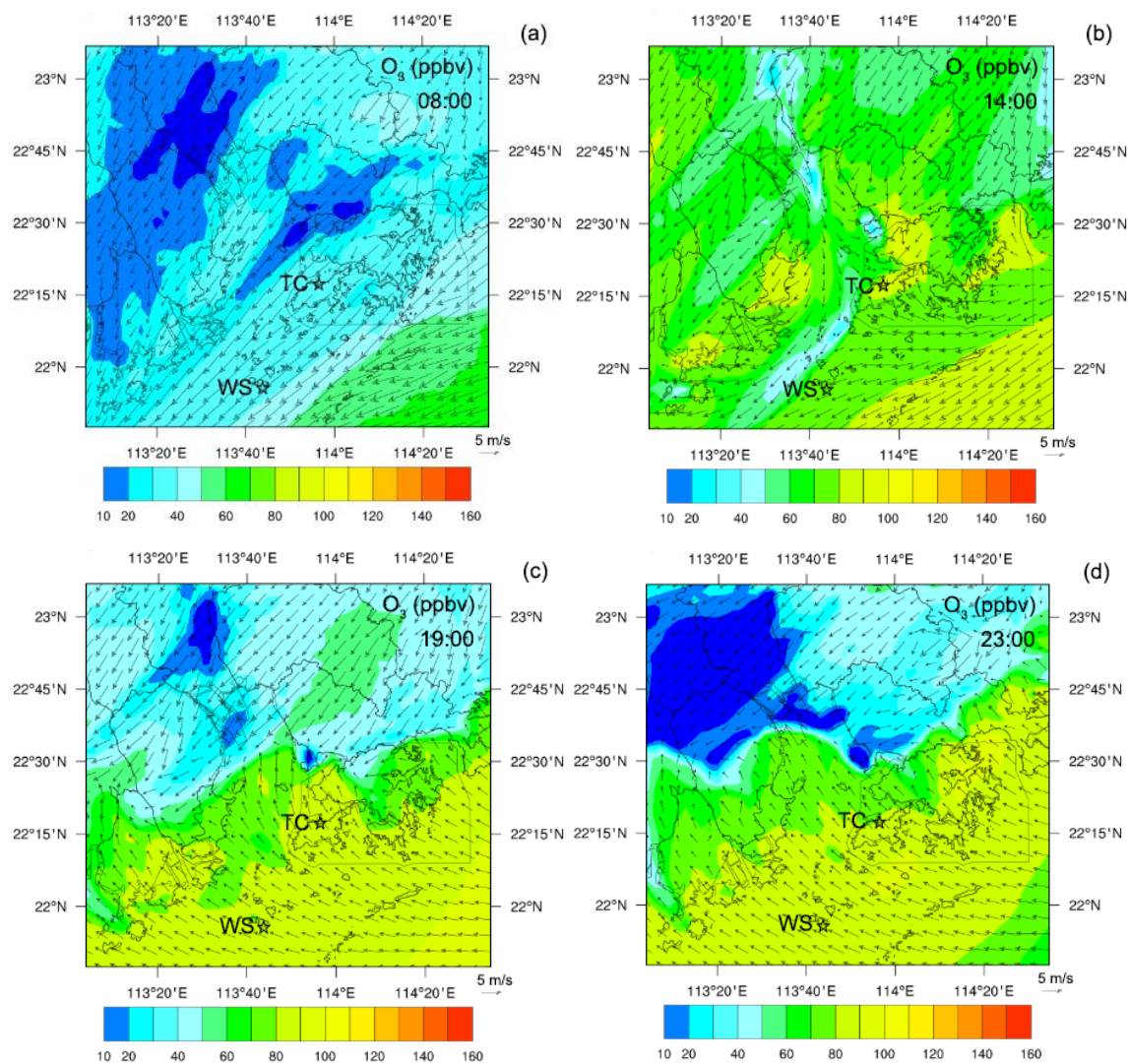


**Figure 8.** Spatial distribution of  $O_3$  at 08:00 (a), 14:00 (b), 19:00 (c) and 23:00 (d) on 3 October, taken as an example of the “SLB” interaction pattern. Arrows in the figure represent the surface wind field.

#### 4. Conclusions

Coastal regions with dense population, economic prosperity and environmental pollution are common in the world. This study provided an overview of  $O_3$  pollution in warm seasons around a coastal region of SCS, focusing on the influences of interactions between marine and continental atmospheres on air quality in this subtropical region. The concurrent measurements of primary and secondary air pollutants at TC (a continental site) and WS (a marine site) from August to November 2013 indicated that  $O_3$  was much higher at WS than that at TC, contrary to the more abundant primary air pollutants at TC. At the two sites,  $O_3$  episodes and near- $O_3$  episodes were frequently observed, which were closely associated with

1 continental anticyclone, tropical cyclone and SLB. In addition to high temperature, strong  
2 solar radiation and weak wind, the aforementioned meteorological conditions all favored the  
3 transport of polluted air masses from continental areas to SCS, during which the air pollutants  
4 were transformed with the aging of air masses. After arriving in SCS, the land-originated air  
5 pollutants further involved in intensive photochemical reactions with the trait of low NO  
6 titration to O<sub>3</sub> and high O<sub>3</sub> production rate, leading to higher O<sub>3</sub> level in marine atmosphere  
7 (WS) than that in coastal cities (TC). In addition to the continental outflow that aggravated O<sub>3</sub>  
8 pollution over SCS, SLB as a common interaction in coastal areas also often facilitated the  
9 recirculation of O<sub>3</sub> formed over SCS to the continental areas, building up O<sub>3</sub> concentration in  
10 coastal cities under sea breeze. The findings can be extended to other similar regions to  
11 advance our understanding of O<sub>3</sub> pollution.

## 12 **Acknowledgements**

13 This project was supported by the Natural Science Foundation of China (Grant No.  
14 41275122), the Research Grants Council (RGC) of the Hong Kong Government of Special  
15 Administrative Region (PolyU5154/13E, PolyU152052/14E, PolyU152052/16E and  
16 CRF/C5004-15E), the Guangdong special fund for science and technology development  
17 (2017B020216007), and partly by the Hong Kong PolyU internal grant (G-SB63, 1-BBW4  
18 and 4-ZZFW). The authors thank HKEPD for provision of the air quality and meteorological  
19 data at TC site, and are grateful to Po On Commercial Association Wan Ho Kan Primary  
20 School at Tung Chung and the National Marine Environmental Monitoring Station at  
21 Wanshan Island for their generous support on the field study. Contributions to field  
22 measurements by Kalam Cheung, Dawei Wang, Bo Liu, Nan Wang, Jiamin Ou, Huanghuang  
23 Yan and Xiaoxin Fu are also highly appreciated. The authors also gratefully acknowledge the  
24 NOAA Air Resources Laboratory (ARL) for the provision of the HYSPLIT transport and  
25 dispersion model and/or READY website (<http://www.ready.noaa.gov>), and Prof. Tao  
26 Wang's group of The Hong Kong Polytechnic University for the provision of the average  
27 diurnal profiles of HONO at TC and HT.

## 28 **References**

29 Adame, J. A., Serrano, E., Bolívar, J. P., and de la Morena, B. A.: On the Tropospheric  
30 Ozone Variations in a Coastal Area of Southwestern Europe under a Mesoscale Circulation,

1 Journal of Applied Meteorology and Climatology, 49, 748-759, 10.1175/2009jamc2097.1,  
2 2010.

3 Bell, M. L., Goldberg, R., Hogrefe, C., Kinney, P. L., Knowlton, K., Lynn, B., Rosenthal, J.,  
4 Rosenzweig, C., and Patz, J. A.: Climate change, ambient ozone, and health in 50 US cities,  
5 Climatic Change, 82(1-2), 61-76, 2007.

6 Cabaraban, M. T. I., Kroll, C. N., Hirabayashi, S., and Nowak, D. J.: Modeling of air  
7 pollutant removal by dry deposition to urban trees using a WRF/CMAQ/i-Tree Eco coupled  
8 system, Environmental pollution, 176, 123-133, 2013.

9 Chan, C. Y.: Effects of Asian air pollution transport and photochemistry on carbon monoxide  
10 variability and ozone production in subtropical coastal south China, Journal of Geophysical  
11 Research, 107, 10.1029/2002jd002131, 2002.

12 Cheng, H., Guo, H., Saunders, S., Lam, S., Jiang, F., Wang, X., Simpson, I., Blake, D., Louie,  
13 P., and Wang, T.: Assessing photochemical ozone formation in the Pearl River Delta with a  
14 photochemical trajectory model, Atmospheric Environment, 44, 4199-4208, 2010b.

15 Cheng, H., Guo, H., Wang, X., Saunders, S. M., Lam, S. H. M., Jiang, F., Wang, T., Ding, A.,  
16 Lee, S., and Ho, K.: On the relationship between ozone and its precursors in the Pearl River  
17 Delta: application of an observation-based model (OBM), Environmental Science and  
18 Pollution Research, 17, 547-560, 2010a.

19 Cui, J., Deolal, S. P., Sprenger, M., Henne, S., Staehelin, J., Steinbacher, M., and Nedelec, P.:  
20 Free tropospheric ozone changes over Europe as observed at Jungfraujoch (1990-2008): An  
21 analysis based on backward trajectories, Journal of Geophysical Research - Atmospheres,  
22 116, 2011.

23 Derwent, R. G., Manning, A. J., Simmonds, P. G., Spain, T. G., and O'Doherty, S.: Analysis  
24 and interpretation of 25 years of ozone observations at the Mace Head Atmospheric Research  
25 Station on the Atlantic Ocean coast of Ireland from 1987 to 2012, Atmospheric Environment,  
26 80, 361-368, 10.1016/j.atmosenv.2013.08.003, 2013.

27 Ding, A. J., Wang, T., Zhao, M., Wang, T. J., and Li, Z. K.: Simulation of sea-land breezes  
28 and a discussion of their implications on the transport of air pollution during a multi-day  
29 ozone episode in the Pearl River Delta of China, Atmospheric Environment, 38, 6737-6750,  
30 10.1016/j.atmosenv.2004.09.017, 2004.



1 Ding, A. J., Wang, T., Thouret, V., Cammas, J. P., and Nedelec, P.: Tropospheric ozone  
2 climatology over Beijing: analysis of aircraft data from the MOZAIC program, *Atmospheric*  
3 *Chemistry and Physics*, 8, 1-13, 2008.

4 Ding, A. J., Fu, C. B., Yang, X. Q., Sun, J. N., Zheng, L. F., Xie, Y. N., Herrmann, E., Nie,  
5 W., Petäjä T., Kerminen, V. M., and Kulmala, M.: Ozone and fine particle in the western  
6 Yangtze River Delta: An overview of 1 yr data at the SORPES station, *Atmospheric*  
7 *Chemistry and Physics*, 13, 5813-5830, 10.5194/acp-13-5813-2013, 2013b.

8 Ding, A. J., Wang, T., and Fu, C. B.: Transport characteristics and origins of carbon  
9 monoxide and ozone in Hong Kong, South China, *Journal of Geophysical Research -*  
10 *Atmospheres*, 118, 9475-9488, 2013a.

11 Draxler, R. R., and Rolph, G. D.: HYSPLIT (HYbrid Single-Particle Lagrangian Integrated  
12 Trajectory) Model access via NOAA ARL READY Website  
13 (<http://www.arl.noaa.gov/ready/hysplit4.html>). , NOAA Air Resources Laboratory, Silver  
14 Spring, Maryland, USA, 2003.

15 Dunlea, E. J., Herndon, S. C., Nelson, D. D., Volkamer, R. M., San Martini, F., Sheehy, P.  
16 M., Zahniser, M. S., Shorter, J. H., Wormhoudt, J. C., Lamb, B. K., Allwine, E. J., Gaffney, J.  
17 S., Marley, N. A., Grutter, M., Marquez, C., Blanco, S., Cardenas, B., Retama, A., Villegas,  
18 C. R. R., Kolb, C. E., Molina, L. T., and Molina, M. J.: Evaluation of nitrogen dioxide  
19 chemiluminescence monitors in a polluted urban environment, *Atmospheric Chemistry and*  
20 *Physics*, 7, 2691-2704, DOI 10.5194/acp-7-2691-2007, 2007.

21 Elshorbany, Y. F., Kurtenbach, R., Wiesen, P., Lissi, E., Rubio, M., Villena, G., Gramsch, E.,  
22 Rickard, A. R., Pilling, M. J., and Kleffmann, J.: Oxidation capacity of the city air of  
23 Santiago, Chile, *Atmospheric Chemistry and Physics*, 9(6), 2257-2273, 2009.

24 Fowler, D., Pilegaard, K., Sutton, M. A., Ambus, P., Raivonen, M., Duyzer, J., Simpson, D.,  
25 Fagerli, H., Fuzzi, S., Schjoerring, J. K., Granier, C., Neftel, A., Isaksen, I. S. A., Laj, P.,  
26 Maione, M., Monks, P. S., Burkhardt, J., Daemmgen, U., Neiryneck, J., Personne, E.,  
27 Wichink-Kruit, R., Butterbach-Bahl, K., Flechard, C., Tuovinen, J. P., Coyle, M., Gerosa, G.,  
28 Loubet, B., Altimir, N., Gruenhage, L., Ammann, C., Cieslik, S., Paoletti, E., Mikkelsen, T.  
29 N., Ro-Poulsen, H., Cellier, P., Cape, J. N., Horvath, L., Loreto, F., Niinemets, U., Palmer, P.  
30 I., Rinne, J., Misztal, P., Nemitz, E., Nilsson, D., Pryor, S., Gallagher, M. W., Vesala, T.,  
31 Skiba, U., Brüeggemann, N., Zechmeister-Boltenstern, S., Williams, J., O'Dowd, C., Facchini,

1 M. C., de Leeuw, G., Flossman, A., Chaumerliac, N., and Erisman, J. W.: Atmospheric  
2 composition change: Ecosystems-Atmosphere interactions, *Atmospheric Environment*, 43,  
3 5193-5267, 10.1016/j.atmosenv.2009.07.068, 2009.

4 Guenther, C. C.: Estimates of global terrestrial isoprene emissions using MEGAN (Model of  
5 Emissions of Gases and Aerosols from Nature), *Atmospheric Chemistry and Physics*, 6,  
6 3181-3210, 2006.

7 Guo, H., Jiang, F., Cheng, H. R., Simpson, I. J., Wang, X. M., Ding, A. J., Wang, T. J.,  
8 Saunders, S. M., Wang, T., Lam, S. H. M., Blake, D. R., Zhang, Y. L., and Xie, M.:  
9 Concurrent observations of air pollutants at two sites in the Pearl River Delta and the  
10 implication of regional transport, *Atmospheric Chemistry and Physics*, 9, 7343-7360, 2009.

11 Guo, H., Ling, Z. H., Cheung, K., Jiang, F., Wang, D. W., Simpson, I. J., Barletta, B.,  
12 Meinardi, S., Wang, T. J., Wang, X. M., Saunders, S. M., and Blake, D. R.: Characterization  
13 of photochemical pollution at different elevations in mountainous areas in Hong Kong,  
14 *Atmospheric Chemistry and Physics*, 13, 3881-3898, 10.5194/acp-13-3881-2013, 2013.

15 Guo, H., So, K. L., Simpson, I. J., Barletta, B., Meinardi, S., and Blake, D. R.: C<sub>1</sub>-C<sub>8</sub> volatile  
16 organic compounds in the atmosphere of Hong Kong: Overview of atmospheric processing  
17 and source apportionment, *Atmospheric Environment*, 41(7), 1456-1472, 2007.

18 HKEPD: Air Quality in Hong Kong 2014, available at:  
19 [http://www.aqhi.gov.hk/api\\_history/english/report/files/AQR2014e\\_Update0616.pdf](http://www.aqhi.gov.hk/api_history/english/report/files/AQR2014e_Update0616.pdf), Hong  
20 Kong Environmental Protection Department, 2015.

21 Huang, J. P., Fung, J. C. H., Lau, A. K. H., and Qin, Y.: Numerical simulation and process  
22 analysis of typhoon-related ozone episodes in Hong Kong, *Journal of Geophysical Research*,  
23 110, 10.1029/2004jd004914, 2005.

24 Huang, J. P., Fung, J. C., and Lau, A. K.: Integrated processes analysis and systematic  
25 meteorological classification of ozone episodes in Hong Kong, *Journal of Geophysical  
26 Research - Atmospheres*, 111(D20), 2006.

27 IPCC: Climate Change 2014: Synthesis Report. Contribution of Working Groups I, II and III  
28 to the Fifth Assessment Report of the Intergovernmental Panel on Climate Change, [Core  
29 Writing Team, R.K. Pachauri and L.A. Meyer (eds.)], IPCC, Geneva, Switzerland, 151, 2014.

1 Jenkin, M. E., Saunders, S. M., and Pilling, M. J.: The tropospheric degradation of volatile  
2 organic compounds: A protocol for mechanism development, *Atmospheric Environment*, 31,  
3 81-104, 1997.

4 Jenkin, M. E., Saunders, S. M., Wagner, V., and Pilling, M. J.: Protocol for the development  
5 of the Master Chemical Mechanism, MCM v3 (Part B): tropospheric degradation of aromatic  
6 volatile organic compounds, *Atmospheric Chemistry and Physics*, 3, 181-193, 2003.

7 Jiang, F., Guo, H., Wang, T., Cheng, H., Wang, X., Simpson, I., Ding, A., Saunders, S., Lam,  
8 S., and Blake, D.: An ozone episode in the Pearl River Delta: Field observation and model  
9 simulation, *Journal of Geophysical Research*, 115, D22305, doi:10.1029/2009JD013583,  
10 2010.

11 Jiang, F., Wang, T., Wang, T., Xie, M., and Zhao, H.: Numerical modeling of a continuous  
12 photochemical pollution episode in Hong Kong using WRF-chem, *Atmospheric  
13 Environment*, 42(38), 8717-8727, 2008.

14 Jiang, Y. C., Zhao, T. L., Liu, J., Xu, X. D., Tan, C. H., Cheng, X. H., Bi, X. Y., Gan, J. B.,  
15 You, J. F., and Zhao, S. Z.: Why does surface ozone peak before a typhoon landing in  
16 southeast China? *Atmospheric Chemistry and Physics*, 15, 13331-13338, 10.5194/acp-15-  
17 13331-2015, 2015.

18 He K.: Multi-resolution Emission Inventory for China (MEIC): model framework and 1990-  
19 2010 anthropogenic emissions. In AGU Fall Meeting Abstracts 2012 Dec.

20 Kleffmann, J.: Daytime sources of nitrous acid (HONO) in the atmospheric boundary layer,  
21 *Chemistry and Physical Chemistry*, 8(8), 1137-1144, 2007.

22 Kumar, P., and Imam, B.: Footprints of air pollution and changing environment on the  
23 sustainability of built infrastructure, *Science of the Total Environment*, 444, 85-101,  
24 10.1016/j.scitotenv.2012.11.056, 2013.

25 Kurokawa, J., Ohara, T., Morikawa, T., Hanayama, S., Janssens-Maenhout, G., Fukui, T.,  
26 Kawashima, K., and Akimoto, H.: Emissions of air pollutants and greenhouse gases over  
27 Asian regions during 2000–2008: Regional Emission inventory in ASia (REAS) version 2,  
28 *Atmospheric Chemistry and Physics*, 13(21), 11019-11058, 2013.

29 Lam, S. H. M., Saunders, S. M., Guo, H., Ling, Z. H., Jiang, F., Wang, X. M., and Wang, T.  
30 J.: Modelling VOC source impacts on high ozone episode days observed at a mountain

1 summit in Hong Kong under the influence of mountain-valley breezes, *Atmospheric*  
2 *Environment*, 81, 166-176, 10.1016/j.atmosenv.2013.08.060, 2013.

3 Lefohn, A. S., Shadwick, D., and Oltmans, S. J.: Characterizing changes in surface ozone  
4 levels in metropolitan and rural areas in the United States for 1980-2008 and 1994-2008,  
5 *Atmospheric Environment*, 44, 5199-5210, 2010.

6 Li, J. F., Lu, K. D., Lv, W., Li, J., Zhong, L. J., Ou, Y. B., Chen, D. H., Huang, X., and  
7 Zhang, Y. H.: Fast increasing of surface ozone concentrations in Pearl River Delta  
8 characterized by a regional air quality monitoring network during 2006-2011, *Journal of*  
9 *Environmental Science -China*, 26, 23-36, 2014.

10 Li, Z. Y., Xue, L. K., Yang, X., Zha, Q. Z., Tham, Y. J., Yan, C., Louie, P. K. K., Luk, C. W.  
11 Y., Wang, T., and Wang, W. X.: Oxidizing capacity of the rural atmosphere in Hong Kong,  
12 Southern China, *Science of the Total Environment*, 612, 1114-1122,  
13 10.1016/j.scitotenv.2017.08.310, 2018.

14 Lin, M. Y., Horowitz, L. W., Payton, R., Fiore, A. M., and Tonnesen, G.: US surface ozone  
15 trends and extremes from 1980 to 2014: quantifying the roles of rising Asian emissions,  
16 domestic controls, wildfires, and climate, *Atmospheric Chemistry and Physics*, 17, 2943-  
17 2970, 10.5194/acp-17-2943-2017, 2017.

18 Ling, Z. H., Guo, H., Lam, S., Saunders, S., and Wang, T.: Atmospheric photochemical  
19 reactivity and ozone production at two sites in Hong Kong: Application of a Master Chemical  
20 Mechanism–photochemical box model, *Journal of Geophysical Research - Atmospheres*, 119,  
21 10567-10582, 2014.

22 Ling, Z. H., Guo, H., Zheng, J. Y., Louie, P. K. K., Cheng, H. R., Jiang, F., Cheung, K.,  
23 Wong, L. C., and Feng, X. Q.: Establishing a conceptual model for photochemical ozone  
24 pollution in subtropical Hong Kong, *Atmospheric Environment*, 76, 208-220,  
25 10.1016/j.atmosenv.2012.09.051, 2013.

26 Liu, H., and Chan, J. C. L.: An investigation of air-pollutant patterns under sea–land breezes  
27 during a severe air-pollution episode in Hong Kong, *Atmospheric Environment* 36, 591–601,  
28 2002.

29 Liu, K.-Y., Wang, Z., and Hsiao, L.-F.: A modeling of the sea breeze and its impacts on  
30 ozone distribution in northern Taiwan, *Environmental Modelling & Software*, 17, 21-27,  
31 2002.

1 Lo, J. C. F., Lau, A. K. H., Fung, J. C. H., and Chen, F.: Investigation of enhanced cross-city  
2 transport and trapping of air pollutants by coastal and urban land-sea breeze circulations,  
3 *Journal of Geophysical Research-Atmospheres*, 111, 2006.

4 Lu, K. D., Zhang, Y. H., Su, H., Shao, M., Zeng, L. M., Zhong, L. J., Xiang, Y. R., Chang, C.  
5 C., Chou, C. K. C., and Wahner, A.: Regional ozone pollution and key controlling factors of  
6 photochemical ozone production in Pearl River Delta during summer time, *Science China*  
7 *Chemistry*, 53, 651-663, 10.1007/s11426-010-0055-6, 2010.

8 Lu, X., Chow, K.-C., Yao, T., Lau, A. K. H., and Fung, J. C. H.: Effects of urbanization on  
9 the land sea breeze circulation over the Pearl River Delta region in winter, *International*  
10 *Journal of Climatology*, n/a-n/a, 10.1002/joc.1947, 2009a.

11 Lu, X., Chow, K. C., Yao, T., Fung, J. C. H., and Lau, A. K. H.: Seasonal variation of the  
12 land-sea breeze circulation in the Pearl River Delta region, *Journal of Geophysical Research-*  
13 *Atmospheres*, 114, 2009b.

14 Monks, P. S., Archibald, A. T., Colette, A., Cooper, O., Coyle, M., Derwent, R., Fowler, D.,  
15 Granier, C., Law, K. S., Mills, G. E., Stevenson, D. S., Tarasova, O., Thouret, V., Von  
16 Schneidemesser, E., Sommariva, R., Wild, O., and Williams, M. L.: Tropospheric ozone and  
17 its precursors from the urban to the global scale from air quality to short-lived climate forcer,  
18 *Atmospheric Chemistry and Physics*, 15, 8889-8973, 10.5194/acp-15-8889-2015, 2015.

19 NARSTO: An Assessment of Tropospheric Ozone Pollution-A North American Perspective,  
20 NARSTO Management Office (Envair), Pasco, Washington, 2000.

21 NRC: Rethinking the Ozone Problem in Urban and Regional Air Pollution, National  
22 Research Council, 1991.

23 Parrish, D. D., Trainer, M., Holloway, J. S., Yee, J. E., Warshawsky, M. S., Fehsenfeld, F. C.,  
24 Forbes, G. L., and Moody, J. L.: Relationships between ozone and carbon monoxide at  
25 surface sites in the North Atlantic region, *Journal of Geophysical Research-Atmospheres*, 103,  
26 13357-13376, 1998.

27 Parrish, D. D., Law, K. S., Staehelin, J., Derwent, R., Cooper, O. R., Tanimoto, H., Volz-  
28 Thomas, A., Gilge, S., Scheel, H. E., Steinbacher, M., and Chan, E.: Long-term changes in  
29 lower tropospheric baseline ozone concentrations at northern mid-latitudes, *Atmospheric*  
30 *Chemistry and Physics*, 12, 11485-11504, 2012.

1 Ran, L., Zhao, C. S., Xu, W. Y., Lu, X. Q., Han, M., Lin, W. L., Yan, P., Xu, X. B., Deng, Z.  
2 Z., Ma, N., Liu, P. F., Yu, J., Liang, W. D., and Chen, L. L.: VOC reactivity and its effect on  
3 ozone production during the HaChi summer campaign, *Atmospheric Chemistry and Physics*,  
4 11, 4657-4667, 10.5194/acp-11-4657-2011, 2011.

5 Saunders, S. M., Jenkin, M. E., Derwent, R. G., and Pilling, M. J.: Protocol for the  
6 development of the Master Chemical Mechanism, MCM v3 (Part A): tropospheric  
7 degradation of non-aromatic volatile organic compounds, *Atmospheric Chemistry and*  
8 *Physics*, 3, 161-180, 2003.

9 Seinfeld, J. H., and Pandis, S. N.: *Atmospheric chemistry and physics: from air pollution to*  
10 *climate change*, John Wiley & Sons, 2016.

11 Shindell, D., Kuylensstierna, J. C. I., Vignati, E., van Dingenen, R., Amann, M., Klimont, Z.,  
12 Anenberg, S. C., Muller, N., Janssens-Maenhout, G., Raes, F., Schwartz, J., Faluvegi, G.,  
13 Pozzoli, L., Kupiainen, K., Hoglund-Isaksson, L., Emberson, L., Streets, D., Ramanathan, V.,  
14 Hicks, K., Oanh, N. T. K., Milly, G., Williams, M., Demkine, V., and Fowler, D.:  
15 Simultaneously Mitigating Near-Term Climate Change and Improving Human Health and  
16 Food Security, *Science*, 335, 183-189, 10.1126/science.1210026, 2012.

17 Simpson, I. J., Blake, N. J., Barletta, B., Diskin, G. S., Fuelberg, H. E., Gorham, K., Huey, L.  
18 G., Meinardi, S., Rowland, F. S., Vay, S. A., Weinheimer, A. J., Yang, M., and Blake, D. R.:  
19 Characterization of trace gases measured over Alberta oil sands mining operations: 76  
20 speciated C-2-C-10 volatile organic compounds (VOCs), CO<sub>2</sub>, CH<sub>4</sub>, CO, NO, NO<sub>2</sub>, NO<sub>y</sub>, O<sub>3</sub>  
21 and SO<sub>2</sub>, *Atmospheric Chemistry and Physics*, 10, 11931-11954, 2010.

22 Skamarock, W. C., Klemp, J. B., Dudhia, J., Gill, D. O., Barker, D. M., Duda, M. G, Huang,  
23 X.-Y., Wang, W., and Powers, J. G.: A Description of the Advanced Research WRF Version  
24 3. NCAR Tech. Note NCAR/TN-475+STR, 113 pp. doi:10.5065/D68S4MVH, 2008.

25 Stein, A.F., Draxler, R.R, Rolph, G.D., Stunder, B.J.B., Cohen, M.D., and Ngan, F.: NOAA's  
26 HYSPLIT atmospheric transport and dispersion modeling system, *Bulletin of American*  
27 *Meteorological Society*, 96, 2059-2077, 2015.

28 Sun, L., Xue, L. K., Wang, T., Gao, J., Ding, A. J., Cooper, O. R., Lin, M. Y., Xu, P. J.,  
29 Wang, Z., Wang, X. F., Wen, L., Zhu, Y. H., Chen, T. S., Yang, L. X., Wang, Y., Chen, J. M.,  
30 and Wang, W. X.: Significant increase of summertime ozone at Mount Tai in Central Eastern

1 China, *Atmospheric Chemistry and Physics*, 16, 10637-10650, 10.5194/acp-16-10637-2016,  
2 2016.

3 Velchev, K., Cavalli, F., Hjorth, J., Marmer, E., Vignati, E., Dentener, F., and Raes, F.:  
4 Ozone over the Western Mediterranean Sea – results from two years of shipborne  
5 measurements, *Atmospheric Chemistry and Physics*, 11, 675-688, 10.5194/acp-11-675-2011,  
6 2011.

7 Wang, N., Guo, H., Jiang, F., Ling, Z. H., and Wang, T.: Simulation of ozone formation at  
8 different elevations in mountainous area of Hong Kong using WRF-CMAQ model, *Science*  
9 *of the Total Environment*, 505, 939-951, 2015.

10 Wang, T., LAM, K. S., and LEE, A. S. Y.: Meteorological and Chemical Characteristics of  
11 the Photochemical Ozone Episodes Observed at Cape D’Aguilar in Hong Kong, *Journal of*  
12 *Applied Meteorology*, 30, 1167-1178, 1998.

13 Wang, T., Guo, H., Blake, D. R., Kwok, Y. H., Simpson, I. J., and Li, Y. S.: Measurements of  
14 Trace Gases in the Inflow of South China Sea Background Air and Outflow of Regional  
15 Pollution at Tai O, Southern China, *Journal of Atmospheric Chemistry*, 52, 295-317,  
16 10.1007/s10874-005-2219-x, 2005.

17 Wang, T., Wei, X. L., Ding, A. J., Poon, C. N., Lam, K. S., Li, Y. S., Chan, L. Y., and Anson,  
18 M.: Increasing surface ozone concentrations in the background atmosphere of Southern China,  
19 1994-2007, *Atmospheric Chemistry and Physics*, 9, 6217-6227, 2009.

20 Wang, Y., Guo, H., Zou, S., Lyu, X., Wang, H., Ling, Z., and Cheng, H.: Ground level O<sub>3</sub>  
21 photochemistry over South China Sea: Application of a near-explicit chemical mechanism  
22 box model, *Environmental Pollution*, under revision, 2017b.

23 Wang, Y., Wang, H., Guo, H., Lyu, X., Cheng, H., Ling, Z., Louie, P. K. K., Simpson, I. J.,  
24 Meinardi, S., and Blake, D. R.: Long term O<sub>3</sub>-precursor relationships in Hong Kong: Field  
25 observation and model simulation, *Atmospheric Chemistry and Physics*, 17(18), 10919-  
26 10935, 2017a.

27 Wei, X., Lam, K.-S., Cao, C., Li, H., and He, J.: Dynamics of the Typhoon Haitang Related  
28 High Ozone Episode over Hong Kong, *Advances in Meteorology*, 2016, 1-12,  
29 10.1155/2016/6089154, 2016.

1 WHO: Health aspects of air pollution with particulate matter, ozone and nitrogen dioxide:  
2 report on a WHO working group, Bonn, Germany 13-15 January 2003, World Health  
3 Organization, 2003.

4 Willmott, C. J.: Some comments on the evaluation of model performance, *Bulletin of the*  
5 *American Meteorological Society*, 63(11), 1309-1313, 1982.

6 Xu, X., Lin, W., Wang, T., Yan, P., Tang, J., Meng, Z., and Wang, Y.: Long-term trend of  
7 surface ozone at a regional background station in eastern China 1991-2006: enhanced  
8 variability, *Atmospheric Chemistry and Physics*, 8, 2595-2607, 2008.

9 Xu, Z., Wang, T., Wu, J., Xue, L., Chan, J., Zha, Q., Zhou, S., Louie, P.K.K., and Luk, C. W.:  
10 Nitrous acid (HONO) in a polluted subtropical atmosphere: Seasonal variability, direct  
11 vehicle emissions and heterogeneous production at ground surface, *Atmospheric environment*,  
12 106, 100-109, 2015.

13 Xue, L. K., Wang, T., Louie, P. K. K., Luk, C. W. Y., Blake, D. R., and Xu, Z.: Increasing  
14 External Effects Negate Local Efforts to Control Ozone Air Pollution: A Case Study of Hong  
15 Kong and Implications for Other Chinese Cities, *Environmental Science and Technology*, 48,  
16 10769-10775, 10.1021/es503278g, 2014.

17 Xue, L., Gu, R., Wang, T., Wang, X., Saunders, S., Blake, D., Louie, P.K.K., Luk, C.W.Y.,  
18 Simpson, I., Xu, Z., Wang, Z., Gao Y., Lee, S., Mellouki, A., and Wang, W.: Oxidative  
19 capacity and radical chemistry in the polluted atmosphere of Hong Kong and Pearl River  
20 Delta region: analysis of a severe photochemical smog episode, *Atmospheric Chemistry and*  
21 *Physics*, 16, 9891-9903, 2016.

22 Yang, J. X., Lau, A. K. H., Fung, J. C. H., Zhou, W., and Wenig, M.: An air pollution episode  
23 and its formation mechanism during the tropical cyclone Nuri's landfall in a coastal city of  
24 south China, *Atmospheric Environment*, 54, 746-753, 10.1016/j.atmosenv.2011.12.023, 2012.

25 Yin, L. H.: Analysis of Meteorological Criteria Leading to Tropical Cyclone Related Ozone  
26 Episodes in Hong Kong, PhD, HKUST, 2004.

27 Zha, Q.: Measurement of nitrous acid (HONO) and the implications to photochemical  
28 pollution (MPhil dissertation, The Hong Kong Polytechnic University), 2015.

29 Zhang, M., and Zhang, L.: Study of the sea-land breeze system in Hong Kong, *Hong Kong*  
30 *Meteorological Society Bulletin*, 22-42, 1997.



1 Zhang, Q., Yuan, B., Shao, M., Wang, X., Lu, S., Lu, K., Wang, M., Chen, L., Chang, C. C.,  
2 and Liu, S. C.: Variations of ground-level O<sub>3</sub> and its precursors in Beijing in summertime  
3 between 2005 and 2011, *Atmospheric Chemistry and Physics*, 14, 6089-6101, 10.5194/acp-  
4 14-6089-2014, 2014.

5 Zheng, J. Y., Zhong, L. J., Wang, T., Louie, P. K. K., and Li, Z. C.: Ground-level ozone in  
6 the Pearl River Delta region: Analysis of data from a recently established regional air quality  
7 monitoring network, *Atmospheric Environment*, 44, 814-823, 2010.

8

9